

Phase transitions in the pseudogap Anderson and Kondo models: Critical dimensions, renormalization group, and local-moment criticality

Lars Fritz and Matthias Vojta

Institut für Theorie der Kondensierten Materie, Universität Karlsruhe, 76128 Karlsruhe, Germany

(Dated: October 15, 2004)

The pseudogap Kondo problem, describing quantum impurities coupled to fermionic quasiparticles with a pseudogap density of states, $\rho(\omega) \propto |\omega|^r$, shows a rich zero-temperature phase diagram, with different screened and free moment phases and associated transitions. We analyze both the particle-hole symmetric and asymmetric cases using renormalization group techniques. In the vicinity of $r = 0$, which plays the role of a lower-critical dimension, an expansion in the Kondo coupling is appropriate. In contrast, $r = 1$ is the upper-critical dimension in the absence of particle-hole symmetry, and here insight can be gained using an expansion in the hybridization strength of the Anderson model. As a by-product, we show that the particle-hole symmetric strong-coupling fixed point for $r < 1$ is described by a resonant level model, and corresponds to an intermediate-coupling fixed point in the renormalization group language. Interestingly, the value $r = 1/2$ plays the role of a second lower-critical dimension in the particle-hole symmetric case, and there we can make progress by a novel expansion performed around a resonant level model. The different expansions allow a complete description of all critical fixed points of the models and can be used to compute a variety of properties near criticality, describing universal local-moment fluctuations at these impurity quantum phase transitions.

I. INTRODUCTION

Non-trivial fixed points and associated phase transitions in quantum impurity problems have been subject of considerable interest in recent years, with applications for impurities in correlated bulk systems, in transport through nanostructures, and for strongly correlated lattice models in the framework of dynamical mean-field theory. Many of those impurity phase transitions occur in variations of the well-known Kondo model¹ which describes the screening of localized magnetic moments by metallic conduction electrons. A paradigmatic example of an intermediate-coupling impurity fixed point can be found in the two-channel Kondo effect.

Non-metallic hosts, where the fermionic bath density of states (DOS) vanishes at the Fermi level, offer a different route to unconventional impurity physics. Of particular interest is the Kondo effect in so-called pseudogap systems^{2,3,4,5,6,7,8}, where the fermionic bath density of states follows a power law at low energies, $\rho(\omega) \propto N_0|\omega|^r$ ($r > 0$). Such a behavior arises in semimetals, in certain zero-gap semiconductors, and in systems with long-range order where the order parameter has nodes at the Fermi surface, e.g., p - and d -wave superconductors ($r = 2$ and 1). Indeed, in d -wave high- T_c superconductors non-trivial Kondo-like behavior has been observed associated with the magnetic moments induced by non-magnetic Zn impurities^{9,10}. Note that the limit $r \rightarrow \infty$ corresponds to a system with a hard gap.

The pseudogap Kondo problem has attracted substantial attention during the last decade. A number of studies^{2,3,4} employed a slave-boson large- N technique; significant progress and insight came from numerical renormalization group (NRG) calculations^{5,6,7} and the local moment approach⁸. It was found that a zero-temperature phase transition occurs at a critical Kondo

coupling, J_c , below which the impurity spin is unscreened even at lowest temperatures. Also, the behavior depends sensitively on the presence or absence of particle-hole (p-h) asymmetry, which can arise, e.g., from a band asymmetry at high energies or a potential scattering term at the impurity site. A comprehensive discussion of possible fixed points and their thermodynamic properties has been given in Ref. 6 based on the NRG approach.

Until recently, analytical knowledge about the critical properties of the pseudogap Kondo transition was limited. Previous works employed a weak-coupling renormalization group (RG) method, based on an expansion in the dimensionless Kondo coupling $j = N_0 J_K$. It was found that an unstable RG fixed point exists at $j = r$, corresponding to a continuous phase transition between the free and screened moment phases². Thus, the perturbative computation of critical properties within this approach is restricted to small r . Interestingly, the NRG studies⁶ showed that the fixed-point structure changes at $r = r^* \approx 0.375$ and also at $r = \frac{1}{2}$, rendering the relevant case of $r = 1$ inaccessible from weak coupling. In the p-h symmetric case, for $r \geq \frac{1}{2}$ the phase transition was found to disappear, and the impurity is always unscreened independent of the value of J_K . In contrast, in the asymmetric case the phase transition is present for arbitrary $r > 0$. Numerical calculations^{6,7} indicated that the critical fluctuations in the p-h asymmetric case change their character at $r = 1$: whereas for $r < 1$ the exponents take non-trivial r -dependent values and obey hyperscaling, exponents are trivial for $r > 1$ and hyperscaling is violated. These findings suggest to identify $r = 1$ as upper-critical “dimension” of the problem, whereas $r = 0$ plays the role of a lower-critical “dimension”. As known, e.g., from the critical theory of magnets¹¹, the description of the transitions using perturbative RG requires different theoretical formulations near the upper-critical and lower-critical

dimensions, i.e., the ϕ^4 theory and the non-linear sigma model in the magnetic case.

In this paper, we provide a comprehensive analytical account of the phase transitions in the pseudogap Anderson and Kondo models, including the proper theories for the critical “dimensions”. This is made possible by working with the Anderson instead of the Kondo model – the degrees of freedom of the Anderson model turn out to provide a natural description of the low-energy physics at the quantum phase transitions near $r = \frac{1}{2}$ as well as close to and above $r = 1$. We shall consider epsilon-type expansions in the hybridization, the on-site energy, and the interaction strength. Those expansions lead to different theories for the p-h symmetric and asymmetric cases. Interestingly, in the pseudogap Kondo model the phase transitions near the lower-critical and upper-critical dimension are not adiabatically connected, as the fixed point structure changes both at $r = r^*$ and $r = \frac{1}{2}$. Thus the present quantum impurity problem has a more complicated flow structure than the critical theory of magnets, where the $(2 + \epsilon)$ and $(4 - \epsilon)$ expansions are believed to describe the same critical fixed point.

In the p-h symmetric case of the pseudogap Kondo problem the line of non-trivial phase transitions terminates at *two lower-critical dimensions* (!), $r = 0$ and $r = \frac{1}{2}$. Near $r = \frac{1}{2}$ we find an expansion around a non-interacting resonant level model, together with perturbative RG, to provide access to the critical fixed point, with the expansion being controlled in the small parameter $(\frac{1}{2} - r)$, see Sec. IV. Interestingly, the weak-coupling expansion for the Kondo model, presented in Sec. III, provides a different means to access the same critical fixed point, but with the small parameter being r ; the two expansions can be expected to match.

In the p-h asymmetric case an expansion can be done in the hybridization around the valence-fluctuation point of the Anderson model. Bare perturbation theory is sufficient for all $r > 1$; for $r < 1$ a perturbative RG procedure is required to calculate critical properties, with the expansion being controlled in the small parameter $(1 - r)$. In particular, this identifies $r = 1$ as the upper-critical dimension of the (asymmetric) pseudogap Kondo problem, and consequently observables acquire logarithmic corrections for $r = 1$. A brief account on the p-h asymmetric case and the expansion around $r = 1$ has been given in a recent paper¹². We note that the flow of the asymmetric Anderson model in the metallic case, $r = 0$, was discussed by Haldane¹³: here all initial parameter sets with finite hybridizations flow towards the strong-coupling (singlet) fixed point.

For all cases listed above, we show that the critical properties of the Anderson and Kondo models are identical, and we calculate various observables in renormalized perturbation theory. To label the fixed points, we will follow the notation of Ref. 6.

Before continuing, we emphasize that standard tools for metallic Kondo models, such as bosonization, Bethe ansatz, and conformal field theory, are not easily applica-

ble in the present case of a pseudogap density of states, as the problem cannot be described using linearly dispersing fermions in one dimension. Furthermore, integrating out the fermions from the problem, in order to arrive at an effective statistical mechanics model containing impurity degrees of freedom only, cannot be performed easily: the fermionic determinants arising in $(1 + r)$ dimensions cannot be simply evaluated. This implies that the pseudogap Kondo model does *not* map onto a one-dimensional (e.g. Ising) model with long-ranged interactions, in contrast to e.g. the spin-boson model¹⁴. Indeed, the phase transitions in the pseudogap Kondo model and the sub-ohmic spin-boson model are in different universality classes¹⁵. Therefore we believe that our combined RG analysis provides a unique tool for analyzing the pseudogap Kondo problem.

A. Models

The starting point of our discussion will be the single-impurity Anderson model with a pseudogap host density of states, $\mathcal{H} = \mathcal{H}_A + \mathcal{H}_b$:

$$\begin{aligned} \mathcal{H}_A &= \varepsilon_0 f_\sigma^\dagger f_\sigma + U_0 n_{f\uparrow} n_{f\downarrow} + V_0 (f_\sigma^\dagger c_\sigma(0) + \text{h.c.}), \\ \mathcal{H}_b &= \int_{-\Lambda}^{\Lambda} dk |k|^r k c_{k\sigma}^\dagger c_{k\sigma} \end{aligned} \quad (1)$$

where we have represented the bath, \mathcal{H}_b , by linearly dispersing chiral fermions $c_{k\sigma}$, summation over repeated spin indices σ is implied, and $c_\sigma(0) = \int dk |k|^r c_{k\sigma}$ is the conduction electron operator at the impurity site. The spectral density of the $c_\sigma(0)$ fermions follows the power law $|\omega|^r$ below the ultra-violet (UV) cutoff Λ ; details of the density of states at high energies are irrelevant for the discussion in this paper. The four possible impurity states will be labelled with $|\uparrow\rangle$, $|\downarrow\rangle$ for the spin-carrying states, $|e\rangle$ for the empty and $|d\rangle$ for the doubly occupied state. Provided that the conduction band is p-h symmetric, the above model obeys p-h symmetry for $U_0 = -2\varepsilon_0$ – this p-h symmetry can be considered as SU(2) pseudospin, i.e., the full symmetry of the model is $\text{SU}(2)_{\text{spin}} \times \text{SU}(2)_{\text{charge}}$. Asymmetry of the high-energy part of the conduction band has the same net effect as asymmetry of the impurity states; we will always assume that the low-energy part of the band is asymptotically symmetric, i.e., the prefactor of $|\omega|^r$ in the DOS is equal for positive and negative ω .

The transformation

$$\begin{aligned} f_\sigma &\rightarrow f_\sigma^\dagger, \\ c_{k\sigma} &\rightarrow c_{k\sigma}^\dagger \end{aligned} \quad (2)$$

converts all particles into holes and vice versa, formally $\varepsilon_0 \rightarrow -(\varepsilon_0 + U_0)$, $V_0 \rightarrow -V_0$. Physically, the roles of the states $|\uparrow\rangle$ and $|\downarrow\rangle$ are interchanged, as well as the states $|e\rangle$ and $|d\rangle$. It is useful to consider another transformation,

$$f_\uparrow \rightarrow f_\uparrow, \quad f_\downarrow \rightarrow f_\downarrow^\dagger,$$

$$c_{k\uparrow} \rightarrow c_{k\uparrow}, c_{k\downarrow} \rightarrow c_{k\downarrow}^\dagger, \quad (3)$$

which transforms $|\uparrow\rangle \leftrightarrow |d\rangle$, $|\downarrow\rangle \leftrightarrow |e\rangle$. Here, the spinful doublet of impurity states is transformed into the spinless doublet and vice versa, i.e., the two SU(2) sectors are interchanged.

In the so-called Kondo limit of the Anderson model charge fluctuations are frozen out, and the impurity site is mainly singly occupied. Via Schrieffer-Wolff transformation one obtains the standard Kondo model, $\mathcal{H} = \mathcal{H}_K + \mathcal{H}_b$, with

$$\mathcal{H}_K = J_K \mathbf{S} \cdot \mathbf{s}(0) \quad (4)$$

where the impurity spin \mathbf{S} is coupled to the conduction electron spin at site 0, $s_\alpha(0) = c_\sigma^\dagger(0)\sigma_{\sigma\sigma'}^\alpha c_{\sigma'}(0)/2$, and σ^α is the vector of Pauli matrices. The Kondo coupling is related to the parameters of the Anderson model (1) through:

$$J_K = 2V_0^2 \left(\frac{1}{|\varepsilon_0|} + \frac{1}{|U_0 + \varepsilon_0|} \right). \quad (5)$$

The Kondo limit is reached by taking $U_0 \rightarrow \infty$, $\varepsilon_0 \rightarrow -\infty$, $V_0 \rightarrow \infty$, keeping J_K fixed. In the absence of p-h symmetry the Schrieffer-Wolff transformation also generates a potential scattering term in the effective Kondo model¹.

In the absence of an external magnetic field all above models preserve SU(2) spin symmetry. Spin anisotropies turn out to be irrelevant at the critical fixed points, see Appendix D. The effect of a magnetic field will be briefly discussed in Sec. VIII.

B. Summary of results

Our main results are summarized in the RG flow diagrams in Figs. 1 and 2, for the p-h symmetric and asymmetric cases, respectively.

In the symmetric case, the ranges of exponent values $r = 0$, $0 < r < \frac{1}{2}$, $\frac{1}{2} \leq r < 1$, and $r \geq 1$ lead to quite different behavior, and are shown separately in Fig. 1. No transition occurs for $r = 0$: for any non-zero hybridization the flow is towards the metallic Kondo-screened fixed point (SC). This well-known fixed point can be identified as the stable fixed point of a resonant level model; we argue below that this is actually an intermediate-coupling fixed point.

For $0 < r < \frac{1}{2}$, small values of the hybridization leave the impurity spin unscreened provided that $\varepsilon_0 < 0$, i.e., there is a stable local-moment fixed point (LM) corresponding to $\varepsilon = -\infty$, $v = 0$. A transition line at negative ε , with an unstable fixed point (symmetric critical, SCR) at finite v , $|\varepsilon|$, separates the flow towards LM from the flow to the symmetric strong-coupling fixed point (SSC). The strong-coupling fixed point displays its intermediate-coupling properties now in a finite residual entropy and a finite magnetic moment, see Sec. IV B. As $r \rightarrow 0$ the SCR

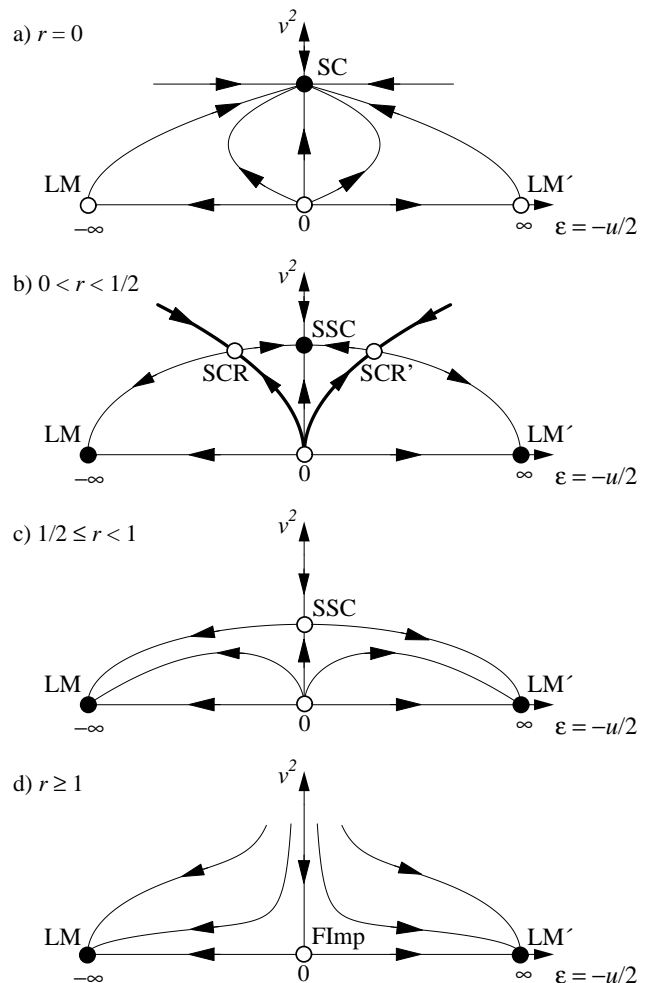


FIG. 1: Schematic RG flow diagrams for the particle-hole symmetric single-impurity Anderson model with a pseudogap DOS, $\rho(\omega) \propto |\omega|^r$. The horizontal axis denotes the renormalized on-site level energy ε (related to the on-site repulsion u by $u = -2\varepsilon$), the vertical axis is the renormalized hybridization v . The thick lines correspond to continuous boundary phase transitions; the full (open) circles are stable (unstable) fixed points, for details see text. All fixed points at non-zero ε have a mirror image at $-\varepsilon$, related by the particle-hole transformation (3). a) $r = 0$, i.e., the familiar metallic case. For any finite v the flow is towards the strong-coupling fixed point (SC), describing Kondo screening. b) $0 < r < \frac{1}{2}$: The local-moment fixed point (LM) is stable, and the transition to symmetric strong coupling (SSC) is controlled by the SCR fixed point. For $r \rightarrow 0$, SCR approaches LM, and the critical behavior at SCR is accessible via an expansion in the Kondo coupling j . In contrast, for $r \rightarrow \frac{1}{2}$, SCR approaches SSC, and the critical behavior can be accessed by expanding in the deviation from SCR, i.e., in $\varepsilon = -u/2$. c) $\frac{1}{2} \leq r < 1$: v is still relevant at $u = 0$. However, SSC is now unstable w.r.t. finite u . At finite v , the transition between the two stable fixed points LM and LM' is controlled by SSC (which is now a critical fixed point!). d) $r \geq 1$: v is irrelevant, and the only transition is a level crossing (with perturbative corrections) occurring at $v = u = 0$, i.e., at the free-impurity fixed point (FImp).

fixed point merges with LM, in a manner characteristic for a lower-critical dimension, i.e., with diverging correlation length exponent. A second critical fixed point SCR' exists for $\varepsilon > 0$ which separates the symmetric strong-coupling phase (SSC) from one with a free charge doublet (LM').

As $r \rightarrow \frac{1}{2}$ the symmetric critical fixed points merge with the strong-coupling one, again in a manner characteristic for a lower-critical dimension. For $r \geq \frac{1}{2}$ the fixed points SCR and SCR' cease to exist; the strong-coupling SSC fixed point becomes infrared unstable, and controls the LM – LM' transition. Finally, the structure of the flow changes again at $r = 1$: for $r \rightarrow 1$ the unstable strong-coupling fixed point (SSC) moves towards $v = 0$, i.e., the free-impurity fixed point (FImp), and for $r \geq 1$ no non-trivial fixed point remains.

For maximal p-h asymmetry, realized in the Anderson model through $U_0 = \infty$, one has to distinguish exponent ranges $r = 0$, $0 < r \leq r^*$, $r^* < r < 1$, and $r \geq 1$. In the metallic case $r = 0$ any non-zero hybridization generates flow to strong coupling with complete screening – the strong-coupling fixed point is the same as in the p-h symmetric situation, as p-h symmetry is marginally irrelevant at strong coupling. For all $r > 0$ the situation is drastically different: small V_0 leaves the moment unscreened, whereas large V_0 directs the flow towards a new, p-h asymmetric, strong-coupling fixed point (ASC). The character of the critical fixed point separating the two phases depends⁶ on r : for $0 < r < r^*$ p-h symmetry is restored, and the critical fixed point is the one of the p-h symmetric model. For $r^* < r < 1$ there is a separate critical fixed point (ACR) which is p-h asymmetric, i.e., located at finite v and ε . For $r \rightarrow 1$ the critical fixed point moves towards $v \rightarrow 0$, and for $r \geq 1$ the phase transition becomes a level crossing (with perturbative corrections), controlled by the valence-fluctuation fixed point (VFI), see Fig. 2.

We finally discuss the general case of finite p-h asymmetry, more details will be given in Sec. VI. Power counting shows that LM (SSC) are always (un)stable w.r.t. p-h asymmetry. The symmetric critical SCR fixed point is stable w.r.t. p-h asymmetry for small r . In contrast, for $r \lesssim \frac{1}{2}$ SCR is unstable towards p-h asymmetry, as it is close to SSC in this regime. This *requires* the existence of a specific r value where this change in character occurs: this is precisely $r = r^* \approx 0.375$ where p-h asymmetry at SCR is marginal⁶. Upon increasing r beyond r^* the p-h asymmetric critical fixed point (ACR) splits off from SCR. In other words, upon approaching r^* from large r the ACR fixed point moves towards small effective p-h asymmetry, and at $r = r^*$ ACR merges into SCR, implying p-h symmetry is dynamically restored. As stated above, the description of ACR using an expansion around VFI consequently breaks down as $r \rightarrow r^{*+}$. Neither from numerics⁶ nor from the present RG are there indications for the existence of a second asymmetric critical fixed point besides ACR; thus, the critical properties for finite p-h asymmetry are always equivalent to the ones of a

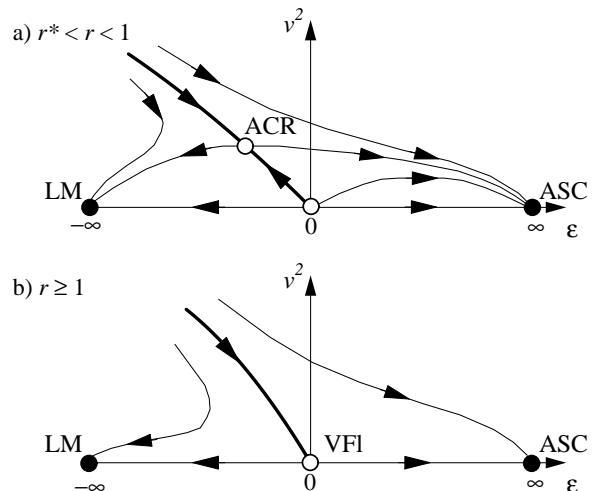


FIG. 2: Schematic RG flow diagram for the maximally particle-hole asymmetric pseudogap Anderson impurity model. The horizontal axis denotes the on-site impurity energy, ε , the vertical axis is the fermionic coupling v , the bare on-site repulsion is fixed at $u_0 = \infty$. The symbols are as in Fig. 1. a) $r^* < r < 1$: v is relevant, and the transition is controlled by an interacting fixed point (ACR). As $r \rightarrow r^* \approx 0.375$, p-h symmetry at the critical fixed point is dynamically restored, and ACR merges into the SCR fixed point of Fig. 1 – this cannot be described using the RG of Sec. V. In the metallic $r = 0$ situation, studied by Haldane¹³, the flow from any point with $v \neq 0$ is towards the screened singlet fixed point with $\varepsilon = \infty$. b) $r \geq 1$: v is irrelevant, and the transition is a level crossing with perturbative corrections, occurring at $v = \varepsilon = 0$, i.e., the valence-fluctuation fixed point (VFI).

model with maximal p-h asymmetry.

Taken together, the above observations show that $r = 0$ plays the role of a lower-critical dimension: as $r \rightarrow 0^+$, the correlation length exponent diverges, and the second-order transition turns into a Kosterlitz-Thouless transition at $r = 0$. Interestingly, in the symmetric case the correlation length exponent also diverges as $r \rightarrow \frac{1}{2}^-$, and the transition between LM and SSC disappears for $r \geq \frac{1}{2}$: $r = \frac{1}{2}$ is a second lower-critical dimension for the p-h symmetric problem. In the asymmetric case, there is a transition between LM and ASC for all $r > 0$, and $r = 1$ is equivalent to the upper-critical dimension, above which the critical fixed point is non-interacting (actually a level crossing).

C. Outline

The rest of this paper is organized as follows: Sec. II introduces the observables to be evaluated in the course of the paper, together with their expected scaling behavior near criticality. In Sec. III we briefly review the standard weak-coupling perturbative RG for the Kondo

model, which is suitable to describe the quantum phase transition for small r . Sec. IV discusses the particle-hole symmetric Anderson model. Starting from the non-interacting case, $\varepsilon_0 = U_0 = 0$, we first discuss the physics of the resulting non-interacting resonant level model – interestingly this can be identified with a stable intermediate-coupling fixed point. We then use a perturbative expansion in U_0 to access the critical fixed points for $r \lesssim \frac{1}{2}$. In Sec. V we turn to the situation with maximal p-h asymmetry, i.e., $U_0 = \infty$, and show that an expansion in the hybridization provides access to the critical properties for $r > 1$ as well as for $r \lesssim 1$. In Sec. VI we consider the case of general p-h asymmetry. Sec. VIII briefly describes the effect of a magnetic field: the pseudogap model is shown to permit a sharp transition as function of a field applied to the impurity for couplings larger than the zero-field critical coupling. In Sec. VII we compare the physics of the Anderson and Kondo models, arguing that the transitions in both models fall in the same universality classes. A brief discussion of applications concludes the paper. All renormalization group calculations will employ the field-theoretic RG scheme¹⁶ together with dimensional regularization and minimal subtraction of poles, with details given in the appendices; one-loop RG results can equivalently be obtained using the familiar momentum-shell method.

II. OBSERVABLES AND SCALING

To establish notations and to pave the way for the RG analysis below, we introduce a few observables together with their expected scaling properties.

A. Susceptibilities

Magnetic susceptibilities are obtained by coupling an external magnetic field to the bulk electronic degrees of freedom in \mathcal{H}_b ,

$$-H_{u\alpha}(x)(c_{\sigma}^{\dagger}\sigma_{\sigma\sigma'}^{\alpha}c_{\sigma'})(x) \quad (6)$$

and to the impurity part \mathcal{H}_A , \mathcal{H}_K ,

$$-H_{\text{imp},\alpha}(f_{\sigma}^{\dagger}\sigma_{\sigma\sigma'}^{\alpha}f_{\sigma'}) , \quad -H_{\text{imp},\alpha}\hat{S}_{\alpha} \quad (7)$$

for the Anderson (1) and Kondo (4) models, respectively. The bulk field H_u varies slowly as function of the space coordinate, and H_{imp} is the magnetic field at the location of the impurity.

With these definitions, a spatially uniform field applied to the whole system corresponds to $H_u = H_{\text{imp}} = H$. Response functions can be defined from second derivatives of the thermodynamic potential, $\Omega = -T \ln Z$, in the standard way¹⁷: $\chi_{u,u}$ measures the bulk response to a field applied to the bulk, $\chi_{\text{imp,imp}}$ is the impurity response to a field applied to the impurity, and $\chi_{u,\text{imp}}$ is the cross-response of the bulk to an impurity field.

The impurity contribution to the total susceptibility is defined as

$$\chi_{\text{imp}}(T) = \chi_{\text{imp,imp}} + 2\chi_{u,\text{imp}} + (\chi_{u,u} - \chi_{u,u}^{\text{bulk}}), \quad (8)$$

where $\chi_{u,u}^{\text{bulk}}$ is the susceptibility of the bulk system in absence of the impurity. For an unscreened impurity spin of size $S = \frac{1}{2}$ we expect $\chi_{\text{imp}}(T \rightarrow 0) = 1/(4T)$ in the low-temperature limit, and this is precisely the result in the whole LM phase. A fully screened moment will be characterized by $T\chi_{\text{imp}} = 0$; note that the SSC fixed point displays a *finite* value of $T\chi_{\text{imp}}$ for $r > 0$. At criticality χ_{imp} does *not* acquire an anomalous dimension¹⁸ (in contrast to χ_{loc} below), because it is a response function associated to the conserved quantity S_{tot} . Thus we expect a Curie law

$$\lim_{T \rightarrow 0} \chi_{\text{imp}}(T) = \frac{C_{\text{imp}}}{T}, \quad (9)$$

where the prefactor C_{imp} is in general a non-trivial universal constant different from the free-impurity value $S(S+1)/3$. Apparently, Eq. (9) can be interpreted as the Curie response of a fractional effective spin¹⁹.

The local impurity susceptibility is given by

$$\chi_{\text{loc}}(T) = \chi_{\text{imp,imp}}, \quad (10)$$

which is equivalent to the zero-frequency impurity spin autocorrelation function. In the unscreened phase we have $\chi_{\text{loc}} \propto 1/T$ as $T \rightarrow 0$; we can consider this as arising from the overlap of the local impurity moment with the total, freely fluctuating, moment of $S = 1/2$, and so write

$$\lim_{T \rightarrow 0} \chi_{\text{loc}}(T) = \frac{m_{\text{loc}}^2}{4T}. \quad (11)$$

The quantity m_{loc} turns out to be a suitable order parameter^{6,7} for the phase transitions between an unscreened and a screened spin: it vanishes continuously as $t \rightarrow 0^-$, where t is the dimensionless measure of the distance to criticality; in the Kondo model $t = (J_K - J_c)/J_c$, whereas in the Anderson model $t = (V_0 - V_{0c})/V_{0c}$. Thus, $T\chi_{\text{loc}}$ is *not* pinned to the value of 1/4 for $t < 0$ (in contrast to $T\chi_{\text{imp}}$). Remarkably, $m_{\text{loc}} = 0$ at the SSC fixed point for $r < 1$, although $T\chi_{\text{imp}} = r/8$ there.

The phase transitions occurring for $0 < r < 1$ are described by interacting fixed points, and thus obey strong hyperscaling properties, including ω/T scaling in dynamical quantities²⁰. For instance, the local dynamic susceptibility will follow a scaling form

$$\chi_{\text{loc}}''(\omega, T) = \frac{\mathcal{B}_1}{\omega^{1-\eta_x}} \Phi_1\left(\frac{\omega}{T}, \frac{T^{1/\nu}}{t}\right) \quad (12)$$

which describes critical local-moment fluctuations, and the local static susceptibility obeys

$$\chi_{\text{loc}}(T) = \frac{\mathcal{B}_2}{T^{1-\eta_x}} \Phi_2\left(\frac{T^{1/\nu}}{t}\right). \quad (13)$$

Here, η_χ is a universal anomalous exponent, which controls the anomalous decay of the two-point correlations of the impurity spin, and $\Phi_{1,2}$ are universal crossover functions (for the specific critical fixed point and for fixed r), whereas $\mathcal{B}_{1,2}$ are non-universal prefactors. Furthermore, ν is the correlation length exponent, describing the flow away from criticality: when the system is tuned through the transition, the characteristic energy scale T^* , above which critical behavior is observed, vanishes as²⁰

$$T^* \propto |t|^\nu; \quad (14)$$

the dynamical critical exponent z can be set to unity in the present $(0+1)$ -dimensional problem. Note that at criticality, $t = 0$, the relation (13) reduces to $\chi_{\text{loc}}(T) \propto T^{-1+\eta_\chi}$.

Hyperscaling can be used to derive relations between critical exponents. The susceptibility exponent η_χ and the correlation length exponent ν of a specific transition are sufficient to determine all critical exponents associated with a local magnetic field⁷. In particular, the $T \rightarrow 0$ local susceptibility away from criticality obeys

$$\begin{aligned} \chi_{\text{loc}}(t > 0) &\propto t^{-\gamma}, \quad \gamma = \nu(1 - \eta_\chi), \\ T\chi_{\text{loc}}(t < 0) &\propto (-t)^{\gamma'}, \quad \gamma' = \nu\eta_\chi, \end{aligned} \quad (15)$$

which can be derived from a scaling ansatz for the impurity part of the free energy⁷. The last relation implies the order parameter vanishing as

$$m_{\text{loc}} \propto (-t)^{\nu\eta_\chi/2}. \quad (16)$$

Note that hyperscaling holds for all critical fixed points of the pseudogap Kondo problem with $0 < r < 1$.

B. Impurity entropy

In general, zero-temperature critical points in quantum impurity models can show a finite residual entropy [in contrast to bulk quantum critical points where the entropy usually vanishes with a power law, $S(T) \propto T^y$]. For the models at hand, the impurity contribution to the low-temperature entropy is obtained by a perturbative evaluation of the thermodynamic potential and taking the temperature derivative. This will yield epsilon-type expansions for the ground state entropy $S_{\text{imp}}(T = 0)$, with explicit results given below.

Note that the impurity part of the thermodynamic potential will usually diverge with the cutoff, i.e., we have $\Omega_{\text{imp}} = E_{\text{imp}} - TS_{\text{imp}}$, where E_{imp} is the non-universal (cutoff-dependent) impurity contribution to the ground-state energy. However, the impurity entropy S_{imp} is fully universal, and the UV cutoff can be sent to infinity *after* taking the temperature derivative of Ω_{imp} .

Thermodynamic stability requires that the total entropy of a system decreases upon decreasing temperature, $\partial_T S(T) > 0$. This raises the question of whether the impurity part of the entropy, S_{imp} has to decrease

under RG flow (which is equivalent to decreasing T). The so-called g -theorem²¹ provides a proof of this conjecture for systems with short-ranged interactions; for most quantum impurity problems this appears to apply. Interestingly, the pseudogap Kondo problem provides an explicit counter-example, as the two critical fixed points obey $S_{\text{SCR}} < S_{\text{ACR}}$, with the RG flow being from SCR to ACR (!), see Sec. V for details. (For another counter-example see Ref. 22.)

C. T matrix

An important quantity in an Anderson or Kondo model is the conduction electron T matrix, describing the scattering of the c electrons off the impurity. For an Anderson model, the T matrix is just given by $T(\omega) = V_0^2 G_f(\omega)$ where G_f is the full impurity f electron Green's function. For a Kondo model, it is useful to define a propagator G_T of the composite operator $T_\sigma = f_\sigma^\dagger f_{\sigma'} c_{\sigma'}$, such that the T matrix is given by $T(\omega) = J_K^2 G_T(\omega)$. As with the local susceptibility, we expect a scaling form of the T matrix spectral density near the intermediate-coupling fixed points similar to Eq. (12). In particular, at criticality a power law occurs:

$$T(\omega) \propto \frac{1}{\omega^{1-\eta_T}}. \quad (17)$$

Remarkably, we will find the *exact* result $\eta_T = 1 - r$ for $r < 1$, i.e., for all *interacting* critical fixed points considered in this paper the T matrix follows $T(\omega) \propto \omega^{-r}$. NRG calculations have found precisely this critical divergence, for both the symmetric and asymmetric critical points^{5,23}. At the trivial fixed points (LM, ASC) the behavior of the T matrix follows from perturbation theory in the hybridization to be $T(\omega) \propto \omega^r$.

Notably, the T matrix can be directly observed in experiments, due to recent advances in low-temperature scanning tunneling microscopy, as has been demonstrated, e.g., with high-temperature superconductors^{23,24,25}.

D. Phase shifts

Fixed points which can be described in terms of free fermions can be characterized by the s -wave conduction electron phase shift, $\delta_0(\omega)$, which can be related to the conduction electron T matrix through $\delta_0(\omega) = \arg T(\omega)$. A decoupled impurity simply has a phase shift $\delta_0 = 0$, whereas a p-h symmetric Kondo-screened impurity in a metallic host has a low-energy phase shift of $\delta_0(\omega) = \frac{\pi}{2} \text{sgn}(-\omega)$. A detailed discussion for the pseudogap model has been given in Ref. 6, in the body of the paper we will simply quote the results.

III. WEAK-COUPLING RG FOR THE KONDO MODEL

In this section we briefly summarize the weak-coupling RG for the pseudogap Kondo model (4), as first discussed by Withoff and Fradkin². Perturbative RG is performed around $J_K = 0$, i.e., the local-moment fixed point (LM): this will allow to access the (p-h symmetric) critical fixed point SCR, which is located close to LM for small DOS exponents r .

A. Lower critical dimension: Expansion around the local-moment fixed point

The RG flow equation for the renormalized Kondo coupling j , to two-loop order, reads²⁶

$$\beta(j) = rj - j^2 + \frac{j^3}{2}. \quad (18)$$

This yields an infrared unstable fixed point at

$$j^* = r + \frac{r^2}{2} + \mathcal{O}(r^3) \quad (19)$$

which controls the transition between the decoupled LM and the Kondo-screened SSC phases. The small- j expansion (18) – which is nothing but the generalization of Anderson poor man’s scaling²⁷ to the pseudogap case – cannot give information about the strong-coupling behavior, and it can only describe critical properties for small r . (In the p-h symmetric case, the fixed point structure does not change within the exponent range $0 < r < \frac{1}{2}$, thus the present expansion is in principle valid up to $r = \frac{1}{2}$.)

Adding a potential scattering term V_0 gives a finite p-h asymmetry. Under RG, we find that V renormalizes to zero for $r > 0$, $\beta(V) = rV$. Thus, within the range of applicability of the weak-coupling RG, p-h asymmetry is irrelevant. (Strictly, this applies for $r < r^*$, see Ref. 6.)

B. Observables near criticality

We quote a few properties of the critical regime which have been determined in Ref. 26. Expanding the beta function (18) around the fixed point value (19) yields the correlation length exponent ν :

$$\frac{1}{\nu} = r - \frac{r^2}{2} + \mathcal{O}(r^3). \quad (20)$$

The low-temperature impurity susceptibility and entropy at criticality are given by

$$T\chi_{\text{imp}} = \frac{1}{4}(1 - r) + \mathcal{O}(r^2), \quad (21)$$

$$S_{\text{imp}} = \ln 2 \left(1 + \frac{3\pi^2}{8} r^3 \right) + \mathcal{O}(r^5). \quad (22)$$

The anomalous exponent of the local susceptibility evaluates to

$$\eta_\chi = r^2 + \mathcal{O}(r^3). \quad (23)$$

A comparison of the above results with numerical data is given in Figs. 3, 5, 6, and 7 below.

Most importantly, the continuous transition controlled by the fixed point (19), which exists only for $r > 0$, evolves smoothly into the Kosterlitz-Thouless transition at $r = 0$, $j = 0$, which separates the antiferromagnetic and the ferromagnetic metallic Kondo model. This is also indicated by the divergence of the correlation length exponent (20) as $r \rightarrow 0^+$. Thus, $r = 0$ can be identified as a lower-critical “dimension” of the pseudogap Kondo problem. It is interesting to compare the present expansion with the $(2+\epsilon)$ expansion for the non-linear sigma model, appropriate for magnets close to the lower-critical dimension. The expansion is done about the ordered magnet, thus the LM phase with $\ln 2$ residual entropy takes the role of the *ordered* state in the pseudogap Kondo problem.

IV. PARTICLE-HOLE SYMMETRIC ANDERSON MODEL

In the following sections of the paper we shift our attention from the Kondo model to the impurity Anderson model with a pseudogap density of states. This formulation will provide new insights into the RG flow and the critical behavior of both the Anderson and Kondo models.

The coupling between impurity and bath is now the Anderson hybridization term, V_0 , which turns out to be marginal in a RG expansion around $V_0 = 0$ for the DOS exponent $r = 1$ (in contrast to the Kondo coupling J_K which is marginal for $r = 0$). As we will show in Sec. V, the Anderson model provides the relevant low-energy degrees of freedom for the p-h asymmetric pseudogap transition near its upper-critical dimension.

Interestingly, also the p-h symmetric version of the Anderson model allows to uncover highly non-trivial physics, in particular the special role played by the DOS exponent $r = \frac{1}{2}$, where the transition disappears in the presence of p-h symmetry. Thus we start our analysis with the particle-hole symmetric Anderson model (1), i.e., we keep $U_0 = -2\varepsilon_0$ and discuss the physics as function of V_0 and ε_0 .

A. Trivial fixed points

For vanishing hybridization, $V_0 = 0$, the symmetric Anderson model (1) features three trivial fixed points: for $\varepsilon_0 < 0$ the ground state is a spinful doublet – this represents the local-moment fixed point (LM). For $\varepsilon_0 > 0$ we find a doublet of states (empty and doubly occupied),

denoted as LM' and related to LM by the p-h transformation (3). Both LM and LM' have a residual entropy of $S_{\text{imp}} = \ln 2$. At $\varepsilon_0 = 0$ a level crossing between the two doublets occurs, i.e., all four impurity states are degenerate – this is the free-impurity fixed point (FImp), with residual entropy $\ln 4$. The impurity spin susceptibilities are

$$T\chi_{\text{imp}} = \begin{cases} 1/4 & \text{LM} \\ 1/8 & \text{FImp} \\ 0 & \text{LM'} \end{cases}, \quad (24)$$

the conduction electron phase shift is zero at all these fixed points. The hybridization term, V_0 , is irrelevant at both the LM and LM' fixed points for $r > 0$, whereas for $r = 0$ it is marginally relevant, as shown by the RG in Sec. III A.

B. Resonant level model: Intermediate-coupling fixed point

It proves useful to discuss the $\varepsilon_0 = U_0 = 0$ case, i.e., the physics on the vertical axis of the flow diagrams in Fig. 1. This non-interacting system is known as resonant level model, as the two spin species are decoupled. The problem can be solved exactly: the f electron self-energy is

$$\Sigma_f = V_0^2 G_{c0} \quad (25)$$

where G_{c0} is the bare conduction electron Green's function at the impurity location $\mathbf{R} = 0$. In the low-energy limit the f electron propagator is then given by

$$G_f(i\omega_n)^{-1} = i\omega_n - iA_0 \text{sgn}(\omega_n) |\omega_n|^r \quad (26)$$

where the $|\omega_n|^r$ self-energy term dominates for $r < 1$, and the prefactor A_0 is

$$A_0 = \frac{\pi V_0^2}{\cos \frac{\pi r}{2}}. \quad (27)$$

Before stating results for observables it is interesting to tackle the problem using RG techniques, with an expansion in the hybridization strength V_0 around the free-impurity fixed point (FImp, $V_0 = 0$). We study the action

$$\mathcal{S} = \int_0^\beta d\tau \left[[\bar{f}_\sigma \partial_\tau f_\sigma + V_0 (\bar{f}_\sigma c_\sigma(0) + \text{c.c.})] + \int_{-\Lambda}^\Lambda dk |k|^r \bar{c}_{k\sigma} (\partial_\tau - k) c_{k\sigma} \right] \quad (28)$$

where $c_\sigma(0)$ is the bath fermion field at the impurity position as above. Power counting w.r.t. the $V_0 = 0$ fixed point, using $\dim[f] = 0$, $\dim[c(0)] = (1+r)/2$, yields

$$\dim[V_0] = \frac{1-r}{2} \equiv \bar{r}, \quad (29)$$

i.e., the hybridization is relevant only for $r < 1$.

To perform RG within the field-theoretic scheme¹⁶, we introduce a renormalized hybridisation v according to $V_0 = (Z_v \mu^{\bar{r}} / \sqrt{Z}) v$, where μ is a renormalization energy scale, and Z_v and Z are the interaction and field renormalization factors. The RG flow equation for v is found to be

$$\beta(v) = -\bar{r}v + v^3. \quad (30)$$

Remarkably, this result is *exact* to all orders in perturbation theory: the cubic term arises from the *only* self-energy diagram of the f fermions, and no vertex renormalizations occur ($Z_v = 1$). This implies that the low-energy physics of the non-interacting resonant level model is controlled by the stable intermediate-coupling fixed point located at

$$v^{*2} = \bar{r} = \frac{1-r}{2} \quad (31)$$

for $0 \leq r < 1$, which also applies to the familiar metallic case $r = 0$.

The intermediate-coupling nature of the stable fixed point, with associated universal properties, is consistent with the results known from the exact solution of the problem, e.g., a universal conduction electron phase shift, a universal crossover in the temperature-dependent susceptibility etc.

We proceed with calculating a number of observables for the pseudogap resonant level model. Interestingly, this can be done in two ways: either (i) via the exact solution of the problem, i.e., by integrating out the c fermions exactly [leading to the propagator (26)], or equivalently (ii) by evaluating perturbative corrections to the FImp fixed point using the RG result (31), utilizing standard renormalized perturbation theory, and noting that all corrections beyond second order in v vanish exactly within this scheme. Details of the calculation are in Appendix A.

We start with evaluating spin susceptibilities – note that we have kept two spin species in the model. The zero-temperature dynamic local susceptibility is proportional to the bubble formed with two f propagators (26),

$$\chi''_{\text{loc}}(\omega) \propto \begin{cases} \omega^{1-2r} & (0 \leq r < 1) \\ \delta(\omega) \frac{\omega}{T} & (r \geq 1) \end{cases}, \quad (32)$$

where the case of $r = \frac{1}{2}$ receives logarithmic corrections, see below. The low-temperature limit of the impurity susceptibility is found to be

$$T\chi_{\text{imp}}(T) = \frac{r}{8}, \quad (33)$$

the impurity entropy is

$$S_{\text{imp}} = 2r \ln 2, \quad (34)$$

where the two last equations are valid for $0 \leq r < 1$; for $r \geq 1$ the resonant level model flows to the free-impurity

fixed point (FImp) with properties listed in Sec. IV A. The conduction electron phase shift near the Fermi level, determined in Ref. 6, is

$$\frac{\delta_0(\omega)}{\text{sgn}(-\omega)} = \begin{cases} (1-r)\frac{\pi}{2} & (0 \leq r < 1) \\ \frac{\pi}{2 \ln|\Lambda/\omega|} & (r = 1) \\ \mathcal{O}(\omega^{r-1}) & (r > 1) \end{cases}. \quad (35)$$

Interestingly, the resonant level model describes a screened impurity only in the metallic case. For the pseudogap case, $r > 0$, Eqs. (33) and (34) show that the impurity is only partially screened: in a model of free fermions we have a residual entropy! We will see below that the resonant level model fixed point (31) can be identified with the symmetric strong-coupling fixed point (SSC) of Gonzalez-Buxton and Ingersent⁶, introduced for the p-h symmetric Kondo and Anderson models.

C. Expansion around the resonant level fixed point

After having analyzed the behavior of the Anderson model in the non-interacting case, we proceed to study the stability of the resonant level fixed point w.r.t. a finite interaction strength U_0 , keeping p-h symmetry. Importantly, this fixed point, characterized by a finite hybridization strength between impurity and bath, is stable for small r [see Eq. (37)]; we conclude that it can be identified with the SSC fixed point of Ref. 6.

Numerical results^{5,6} indicate that the quantum phase transition between LM and SSC disappears as r is increased to $\frac{1}{2}$, where the p-h symmetric critical fixed point (SCR) merges with the SSC fixed point. We shall show that an expansion around the SSC fixed point captures the physics of the SCR fixed point for $r \lesssim \frac{1}{2}$. Thus, this expansion describes *the same* critical fixed point as the weak-coupling expansion of Sec. III, but approaching it from $r = \frac{1}{2}$ instead of $r = 0$. (The r values 0 and $\frac{1}{2}$ are *two* lower-critical dimensions for the p-h symmetric pseudogap Kondo problem.)

The RG expansion below will be performed around an *intermediate-coupling* fixed point, in contrast to most analytical RG calculations which expand around trivial (i.e. weak or strong-coupling) fixed points. Strategically, one could think about a double expansion in V_0 and U_0 . However, this is not feasible, as the marginal dimensions for both couplings are different, $r = 1$ and $r = \frac{1}{2}$, respectively. Therefore we choose to first integrate out the c fermions exactly, and then use standard RG tools for the expansion in U_0 .

Consequently, the starting point is the action

$$\mathcal{S} = \sum_{\omega_n} \bar{f}_\sigma(\omega_n) [iA_0 \text{sgn}(\omega_n) |\omega_n|^r] f_\sigma(\omega_n) \quad (36)$$

$$+ \int_0^\beta d\tau U_0 \left(\bar{f}_\uparrow f_\uparrow - \frac{1}{2} \right) \left(\bar{f}_\downarrow f_\downarrow - \frac{1}{2} \right)$$

where the f fermions are now “dressed” by the conduction lines. A_0 is the non-universal number given in Eq.

(27), and we have assumed $0 < r < 1$. The interaction term has been written in a p-h symmetric form. A note is in order regarding the cutoff: The original model had a UV cutoff Λ , and this sets the upper bound for the $|\omega_n|^r$ behavior of the f propagator (26), i.e., Λ is now the energy cutoff for the spectral density of the f fermions. The RG to be performed below can be understood as progressive reduction of this cutoff (although we will use the field-theoretic scheme where the cutoff is implicitly sent to infinity at an early stage).

Dimensional analysis w.r.t. the $U_0 = 0$ situation, using $\dim[f] = (1-r)/2$, results in

$$\dim[U_0] = 2r - 1 \equiv -\epsilon, \quad (37)$$

hence, for $r > 1/2$ the interaction term is relevant and the SSC fixed point is unstable.

We continue with the RG analysis of (36). To perform a perturbative expansion in U_0 using the field-theoretic scheme¹⁶, we introduce a renormalized field and a dimensionless coupling according to

$$f_\sigma = \sqrt{Z} f_{R\sigma}, \quad (38)$$

$$U_0 = \frac{\mu^{-\epsilon} A_0^2 Z_4}{Z^2} u \quad (39)$$

where μ is a renormalization energy scale as usual, and $(-\epsilon)$ is the bare scaling dimension of U_0 ; we have absorbed the non-universal number A_0 appearing in the dynamic term of the action (36) in order to obtain a universal fixed point value of u .

The complete RG analysis, needed to determine the flow of u , is presented in Appendix B, here we restrict ourselves to the final results. P-h symmetry prohibits the occurrence of even powers of u in the beta function of u , therefore the lowest contributions arise at two-loop order. Remarkably, no singular propagator renormalizations occur, thus

$$Z = 1 \quad (40)$$

to all orders in perturbation theory. The RG flow equation for the renormalized interaction u , arising now only from two-loop vertex renormalizations, is found to be

$$\beta(u) = \epsilon u - \frac{3(\pi - 2 \ln 4)}{\pi^2} u^3. \quad (41)$$

Next-to-leading order contributions would require a four-loop calculation which we do not attempt here. For positive ϵ , i.e., $r < \frac{1}{2}$, Eq. (41) yields a pair of unstable fixed points at finite $|u|$ (in addition to the stable one at $u = 0$); the correlation length exponent of the transition, Eq. (43), diverges as $r \rightarrow \frac{1}{2}^-$. Thus, the behavior *below* $r = \frac{1}{2}$ is similar to the standard behavior *above* a lower-critical dimension (e.g. in the non-linear sigma model for bulk magnet case).

D. $r = 0$

Clearly, the unstable finite- u fixed points predicted by the perturbative RG equation (41) do not necessarily exist for the metallic case $r = 0$, as $\epsilon = 1$ is possibly outside the convergence radius of the expansion. Indeed, the Kondo RG of Sec. III A shows that, at $r = 0$, the LM and LM' fixed points are unstable w.r.t. finite impurity coupling. As the resonant-level fixed point at $u = 0$ is stable, we conclude that the flow is directly from LM (LM') to SC, and SC represents the familiar strong-coupling Kondo fixed point, with complete screening of the spin. The RG flow is in Fig. 1a.

E. $0 < r < \frac{1}{2}$

For r values smaller than $\frac{1}{2}$, both the $v = v^*, u = 0$ fixed point (SSC) and the $v = 0, |\epsilon| = \infty$ fixed points (LM, LM') are stable, and should be separated by critical fixed points. The RG equation (41) yields a pair of infrared unstable fixed points at

$$u^{*2} = \frac{\pi^2}{3(\pi - 2 \ln 4)} \epsilon + \mathcal{O}(\epsilon^2) \quad (42)$$

with $\epsilon = 1 - 2r$. These two fixed points represent SCR and SCR', see the flow diagram in Fig. 1b. Note that p-h symmetry also dictates that the flow trajectories out of the SSC fixed point are horizontal in the u - v^2 diagram. Therefore, close to $r = \frac{1}{2}$ the SCR and SCR' fixed points are completely described by the fixed point coupling values v^* (31) and u^* (42).

F. $\frac{1}{2} \leq r < 1$

For $r > \frac{1}{2}$ ($r = \frac{1}{2}$) the self-interaction u is a (marginally) relevant perturbation at the SSC fixed point, and (41) does not yield additional non-trivial fixed points. As LM and LM' are stable, we can conclude that the flow is from SSC directly towards LM (LM') for positive (negative) U_0 . Hence, SSC has become a critical fixed point, controlling the transition between LM and LM', which occurs at $U_0 = 0$ for any finite V_0 . We shall not consider this transition in greater detail, apart from stating its correlation length exponent, $1/\nu = -\epsilon$. Fig. 1c displays the flow diagram arising from this discussion, being consistent with the numerical results of Ref. 6.

G. $r \geq 1$

The physics of the symmetric Anderson model for $r \geq 1$ is easily discussed: the hybridization term V_0 is irrelevant for all U_0 , Eq. (29). The free-impurity fixed point (FImp) is the only remaining fixed point at $U_0 = 0$. It is unstable w.r.t. finite U_0 , and controls the transition

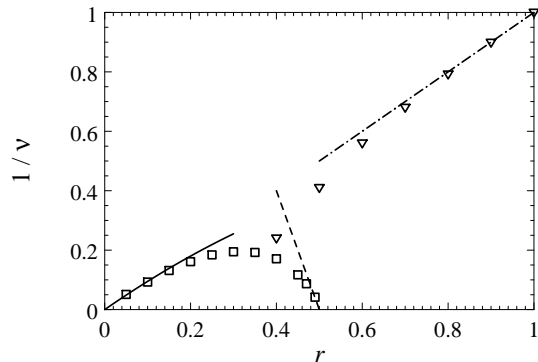


FIG. 3: Inverse correlation length exponent $1/\nu$ obtained from NRG, at both the symmetric (squares) and asymmetric (triangles) critical points, together with the analytical RG results from the expansions in r [Sec. III, Eq. (20), solid], in $(\frac{1}{2} - r)$ [Sec. IV, Eq. (43), dashed], and in $(1 - r)$ [Sec. V, Eq. (72), dash-dot]. The numerical data have been partially extracted from Ref. 7 using hyperscaling relations; for the symmetric model data are from Ref. 5.

between the two stable fixed points LM and LM'. The resulting flow diagram is in Fig. 1d.

H. Observables near criticality

Here we discuss critical properties of the SCR fixed point, the properties of SCR' are identical when translated from spin to charge degrees of freedom. The correlation length exponent follows from expanding the beta function (41) around its fixed-point value:

$$\frac{1}{\nu} = 2 - 4r + \mathcal{O}(\epsilon^2) \quad (43)$$

A comparison with results from NRG is shown in Fig. 3. Close to $r = \frac{1}{2}$, the analytical expression nicely matches the numerical results, however, higher-order corrections in the expansion quickly become important.

We continue with the quantities introduced in Sec. II. As usual for an expansion where the non-linear coupling has an infrared *unstable* fixed point (as occurs above the lower-critical dimension in standard situations), the UV cutoff needs to be kept explicitly, and intermediate quantities will diverge with the UV cutoff (see e.g. the calculation of the impurity entropy). However, these divergences will cancel in the final expressions for universal observables, and this is an important check for the consistency of our calculations.

1. Local susceptibility

The local susceptibility at the SSC fixed point, i.e., at tree level, follows the power law $\chi_{\text{loc}} \propto \omega^{1-2r} = \omega^\epsilon$. To obtain corrections to the tree-level result, one introduces

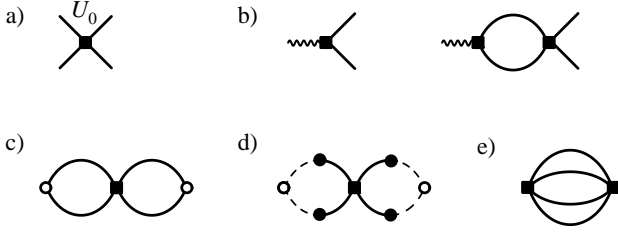


FIG. 4: Feynman diagrams for the symmetric Anderson impurity model, where the expansion is done in U_0 around the resonant level model fixed point. Full lines are *dressed* f_σ propagators with the self-energy arising from the conduction electrons already taken into account, i.e., with the propagator given in Eq. (26). a) Bare interaction vertex U_0 . b) Correlation function involving a composite ($\bar{f}f$) operator (wiggly line), together with the first perturbative correction. c) U_0 correction to the local susceptibility $\chi_{\text{imp,imp}} = \chi_{\text{loc}}$, open circles are sources. d) U_0 correction to $\chi_{u,u}$, which contributes to the Curie term of the impurity susceptibility χ_{imp} . Dashed lines are conduction electron lines, and the full dots are the V_0 vertices. e) U_0^2 contribution to the impurity free energy.

a χ_{loc} renormalization factor, Z_χ , from which one obtains the anomalous exponent according to

$$\eta'_\chi = \beta(u) \left. \frac{d \ln Z_\chi}{du} \right|_{u^*}. \quad (44)$$

Note that $1 - \eta_\chi = \epsilon + \eta'_\chi$, with η_χ defined in Eqs. (12,13), due to the non-trivial structure of the problem already at tree level.

Different ways can be used to determine Z_χ . Realizing that χ_{loc} is a correlation function of a composite ($\bar{f}f$) operator leads to $Z_\chi = Z_2^2$, where Z_2 is the renormalization factor associated with ($\bar{f}f$). Z_2 can be calculated from the correlation function shown in Fig. 4b, which receives a perturbative correction to first order in U_0 . Alternatively, χ_{loc} can be calculated directly, and a single diagram gives a contribution of order U_0 (Fig. 4c). Both ways lead to

$$Z_\chi = 1 + \frac{2u}{\pi\epsilon}, \quad (45)$$

with details given in Appendix B. The result for χ_{loc} is proportional to the non-universal number A_0^{-2} , however, the exponent is universal:

$$\eta'_\chi = \frac{2}{\pi} u^* = 2[3(\pi - 2 \ln 4)]^{-1/2} \sqrt{\epsilon} \quad (46)$$

The local susceptibility thus follows $\chi_{\text{loc}}(T) \propto T^{-1+\eta_\chi}$ with

$$\eta_\chi = 2 - 2r + 2.688 \sqrt{\frac{1}{2} - r} + \mathcal{O}(\epsilon) \quad (47)$$

where the first term contains the tree level expression, and further $\mathcal{O}(\epsilon)$ terms arise from higher-order perturbative corrections. A comparison with NRG results is given in Fig. 5, where good agreement near $r = \frac{1}{2}$ can be observed.

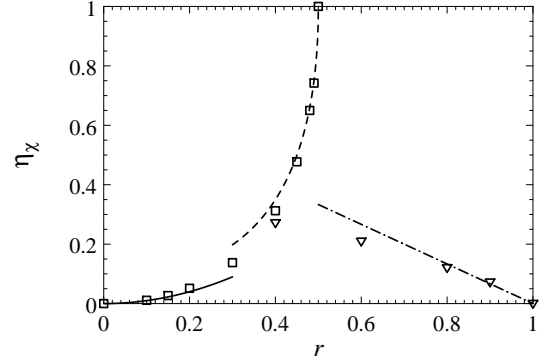


FIG. 5: NRG data⁷ for the local susceptibility exponent, η_χ , defined through $\chi_{\text{loc}} \propto T^{-1+\eta_\chi}$, at both the symmetric (squares) and asymmetric (triangles) critical points, together with the renormalized perturbation theory results from the expansions in r [Sec. III, Eq. (23), solid], in $(\frac{1}{2} - r)$ [Sec. IV, Eq. (47), dashed], and in $(1 - r)$ [Sec. V, Eq. (75), dash-dot].

2. Impurity susceptibility

For the impurity contribution to the uniform susceptibility we expect a Curie law, as discussed in Sec. II. At tree level, a term of Curie form does only arise from $\chi_{u,u}$, with $T\chi_{u,u} = r/8$. Both $\chi_{\text{imp,imp}}$ and $\chi_{u,\text{imp}}$ are less singular for $r < 1$, consistent with $T\chi_{\text{loc}} = 0$, see also Appendix A. Also note that $\chi_{u,u}$ is the only of the three terms where the non-universal number A_0 drops out.

We are interested in corrections to $T\chi_{\text{imp}}$ to lowest non-trivial order in U_0 , and consequently those corrections can only occur in $\chi_{u,u}$. A single diagram contributes to first order in U_0 (Fig. 4d), which gives

$$\Delta\chi_{\text{imp}} = U_0 \frac{V_0^4}{2A_0^4} \left[\int_{-\Lambda}^{\Lambda} dk |k|^r T \sum_n \frac{|\omega_n|^{-2r}}{(i\omega_n - k)^2} \right]^2 \quad (48)$$

The k integral can be performed first, with the UV cutoff sent to infinity, and the frequency summation then leads to

$$\Delta\chi_{\text{imp}} = \frac{1}{T} (1 - 2^{-1-r})^2 \frac{\zeta(1+r)^2}{2\pi^{2(1+r)}} \frac{U_0 T^\epsilon}{A_0^2} \quad (49)$$

In the low-energy limit, the combination $(U_0 T^\epsilon / A_0^2)$ approaches a universal value, the non-universal prefactors V_0 are seen to cancel, and the result has the expected universal Curie form. Introducing the renormalized coupling u we have to leading order in ϵ :

$$\Delta(T\chi_{\text{imp}}) = \left(1 - \frac{1}{2\sqrt{2}}\right)^2 \frac{\zeta(3/2)^2}{2\pi^3} u. \quad (50)$$

Using the fixed point value of u (42), the result for the impurity susceptibility at the SCR fixed point reads

$$T\chi_{\text{imp}} = \frac{r}{8} + 0.1942 \sqrt{\frac{1}{2} - r} + \mathcal{O}(\epsilon) \quad (51)$$

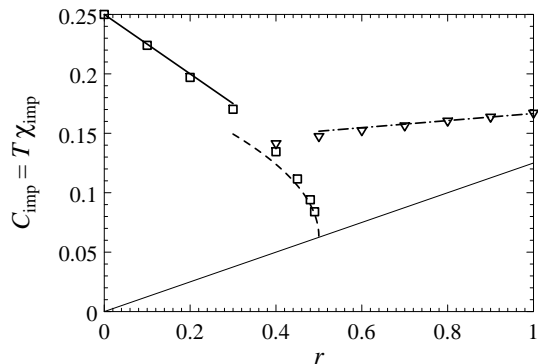


FIG. 6: Numerical data for the impurity susceptibility, $T\chi_{\text{imp}}$, at both the symmetric (squares) and asymmetric (triangles) critical points, together with the renormalized perturbation theory results from the expansions in r [Sec. III, Eq. (21), solid], in $(\frac{1}{2} - r)$ [Sec. IV, Eq. (51), dashed], and in $(1 - r)$ [Sec. V, Eq. (85), dash-dot]. The thin line is the value of the SSC fixed point, $T\chi_{\text{imp}} = r/8$. The numerical data are partially taken from Ref. 6; we have re-calculated the data points near $r = 1$, as the logarithmically slow flow at $r = 1$ complicates the data analysis.

where $r/8$ is the tree level contribution, and the $\mathcal{O}(\epsilon)$ represents higher perturbative terms as above. This result can be nicely compared to NRG data of Ref. 6, see Fig. 6.

3. Impurity entropy

The impurity entropy can be straightforwardly determined from a perturbative expansion of the impurity part of the thermodynamic potential. The lowest correction to the tree-level value $S_{\text{imp}} = 2r \ln 2$ is of order U_0^2 . The corresponding contribution to the thermodynamic potential, Fig. 4e, is given by

$$\Delta\Omega_{\text{imp}} = \frac{U_0^2}{2} \int_0^\beta d\tau G_f^2(\tau) G_f^2(-\tau). \quad (52)$$

Here $G_f(\tau)$ is the fourier-transformed Green's function G_f (26) in the presence of an UV cutoff Λ . Taking the temperature derivative we can write the entropy result as

$$\Delta S_{\text{imp}} = \frac{U_0^2 T^{2\epsilon}}{2A_0^4} \left[\partial_T \int_0^\beta d\tau \bar{G}_f^2(\tau) \bar{G}_f^2(-\tau) \Big|_{r=\frac{1}{2}} \right] \quad (53)$$

where $\bar{G}_f = A_0 G_f$. The prefactor can be expressed in terms of the renormalized coupling u^2 and will be proportional to ϵ at the fixed point. Thus, to leading order the square bracket term can be evaluated at $r = \frac{1}{2}$, and is expected to be a universal, finite number in the limit of $\Lambda \rightarrow \infty$. Unfortunately, we were not able to analytically prove the convergence of the integral as $\Lambda \rightarrow \infty$. We have therefore resorted to a numerical evaluation for finite Λ

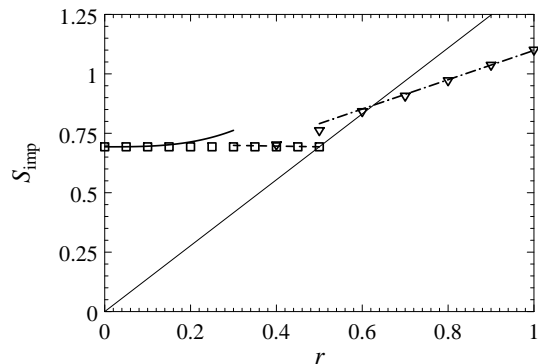


FIG. 7: As Fig. 6, but for the impurity entropy S_{imp} ; the NRG values at the SSC fixed point are hardly distinguishable from $\ln 2$. The perturbative expansions are in Eq. (22) (solid), Eq. (55) (dashed), and Eq. (89) (dash-dot); the thin line is the value of the SSC fixed point, $T\chi_{\text{imp}} = 2r \ln 2$.

and T , with an extrapolation of the result to $\Lambda/T \rightarrow \infty$, and obtained $[\partial_T \dots] = 0.1590 \pm 0.0005$, i.e.,

$$\Delta S_{\text{imp}} = 0.159 \frac{u^2}{2}. \quad (54)$$

Adding the tree-level result and the u^2 correction we obtain

$$S_{\text{imp}} = \ln 2 + (0.03 \pm 0.005) \left(\frac{1}{2} - r \right) + \mathcal{O}(\epsilon^{3/2}). \quad (55)$$

The two expansions for the entropy of the SSC fixed point, (22) and (55), predict a small positive correction to $\ln 2$ for $0 < r < \frac{1}{2}$, as shown in Fig. 7, consistent with the notion that entropy should decrease under RG flow²¹. Results from NRG (Ref. 6 as well as ours) show that the deviation from $\ln 2$ is tiny for all $0 < r < \frac{1}{2}$, which is in principle consistent with the analytical results. [Although we identified signatures of a r^3 correction to $S_{\text{imp}} = \ln 2$ in the small- r regime, the accuracy of our NRG procedure was insufficient to determine the prefactor²⁶.]

4. Conduction electron T matrix

In the Anderson model formulation of the impurity problem, the conduction electron T matrix is directly proportional to the physical f electron propagator. As shown in Appendix B, there are no singular propagator renormalizations in the present problem, $Z = 1$ (40). Thus, from Eq. (26) we have the *exact* result for the exponent of the T matrix,

$$\text{Im}T(\omega) \propto |\omega|^{-r}, \quad (56)$$

which holds at the SCR and SCR' fixed points, and (trivially) also at the SSC fixed point. A result similar to Eq. (56) was derived²⁸ for the SCR fixed point within

the small- r expansion of Sec. III, in agreement with the notion that both expansions describe the same critical fixed point.

V. MAXIMALLY PARTICLE-HOLE ASYMMETRIC ANDERSON MODEL

In this section we consider a different limit of the pseudogap Anderson model (1), namely the model with maximal p-h asymmetry. This means that one of the four possible impurity states will be excluded: with $U_0 \rightarrow \infty$ (keeping ε_0 finite) this is the doubly occupied one, whereas with $\varepsilon_0 \rightarrow -\infty$ (keeping U_0 finite) the empty state is excluded. As these two situations are related by the p-h transformation (2), we will formulate the following for $U_0 \rightarrow \infty$. The Hamiltonian can be written as

$$\mathcal{H} = \varepsilon_0 |\sigma\rangle\langle\sigma| + V_0 [|\sigma\rangle\langle e| c_\sigma(0) + \text{h.c.}] \quad (57)$$

$$+ \int_{-\Lambda}^{\Lambda} dk |k|^r k c_{k\sigma}^\dagger c_{k\sigma}$$

where $|\uparrow\rangle$, $|\downarrow\rangle$, and $|e\rangle$ represent the three allowed impurity states.

We shall show that this infinite- U pseudogap Anderson model has a phase transition between a free-moment and a Kondo-screened phase, which is accessible to perturbative RG techniques near $r = 1$. In particular, $r = 1$ plays the role of the upper-critical dimension. Furthermore, we will argue in Secs. VI and VII that the transitions in both the Anderson and the Kondo model with *finite* p-h asymmetry are in the same universality class, and are described by the RG presented below, provided that $r > r^*$.

A. Trivial fixed points

For vanishing hybridization V_0 , the maximally asymmetric Anderson model features three trivial fixed points: for $\varepsilon_0 < 0$ the ground state is the spinful doublet (LM) with $\ln 2$ entropy. For $\varepsilon_0 > 0$ we have an empty-state singlet, which we can identify with the ASC state of the Kondo model (see below). The doubly occupied singlet state (labelled ASC') is related to ASC by the p-h transformation (2). For $\varepsilon_0 = 0$ we have three degenerate impurity states, we refer to this as the valence-fluctuation fixed point (VFL), with entropy $\ln 3$. The impurity spin susceptibilities are

$$T\chi_{\text{imp}} = \begin{cases} 1/4 & \text{LM} \\ 1/6 & \text{VFL} \\ 0 & \text{ASC} \end{cases} . \quad (58)$$

Again, the conduction electron phase shift is zero at these fixed points due to the vanishing fixed point value of the hybridization. The hybridization term, V_0 , is irrelevant at the ASC fixed point for all r , and irrelevant at LM for $r > 0$.

B. Upper-critical dimension: Expansion around the valence-fluctuation fixed point

In the following we perform an expansion around the VFL fixed point, i.e., around $\varepsilon_0 = 0$, $V_0 = 0$. This will give access to the properties of the ASC fixed point, i.e., a critical fixed point different from the one accessed by the RG calculations in Secs. III and IV.

To represent the three impurity states in the infinite- U Anderson model it is useful to introduce auxiliary fields for pseudo-particles, b_s (for the empty-state singlet) and f_σ (for the spinful doublet). The required Hilbert space constraint $b_s^\dagger b_s + f_\sigma^\dagger f_\sigma = \hat{Q} = 1$ will be implemented using a chemical potential $\lambda_0 \rightarrow \infty$, such that observables $\langle \hat{O} \rangle$ have to be calculated according to^{29,30}

$$\langle \hat{O} \rangle = \lim_{\lambda_0 \rightarrow \infty} \frac{\langle \hat{Q} \hat{O} \rangle_{\lambda_0}}{\langle \hat{Q} \rangle_{\lambda_0}}, \quad (59)$$

where $\langle \dots \rangle_{\lambda_0}$ denotes the thermal expectation value calculated using pseudo-particles in the presence of the chemical potential λ_0 . Clearly, in the limit $\lambda_0 \rightarrow \infty$ the term $\langle \hat{Q} \rangle_{\lambda_0}$ represents the partition function of the physical sector of the Hilbert space times $\exp(-\lambda_0 \beta)$. As detailed in Ref. 26, both numerator *and* denominator of Eq. (59) have to be expanded in the non-linear couplings to the required order when calculating observables; however, the denominator does typically not develop logarithmic singularities at the marginal dimension.

Furthermore, we need to introduce chemical-potential counter-terms which cancel the shift of the critical point occurring in perturbation theory upon taking the limit of infinite UV cutoff. Technically, this shift arises from the real parts of the self-energies of the b_s and f_σ particles. We introduce the counter-terms as additional chemical potential for the auxiliary particles,

$$\delta\lambda_b b_s^\dagger b_s, \quad \delta\lambda_f f_\sigma^\dagger f_\sigma. \quad (60)$$

The $\delta\lambda_{b,f}$ have to be determined order by order in an expansion in V_0 . Note that counter-term contributions in observables in general enter both numerator and denominator in Eq. (59).

The model (57) can then be written in the path integral form

$$\mathcal{S} = \int_0^\beta d\tau \left[\bar{f}_\sigma (\partial_\tau - \varepsilon_0 - \lambda_0 - \delta\lambda_f) f_\sigma \right. \\ \left. + \bar{b}_s (\partial_\tau - \lambda_0 - \delta\lambda_b) b_s \right. \\ \left. + V_0 (\bar{f}_\sigma b_s c_\sigma(0) + \text{c.c.}) \right. \\ \left. + \int_{-\Lambda}^{\Lambda} dk |k|^r \bar{c}_{k\sigma} (\partial_\tau - k) c_{k\sigma} \right] \quad (61)$$

where λ_0 is the chemical potential enforcing the constraint exactly, and the rest of the notation is as above. The counter-terms (60) are determined from the real parts of the self-energies of both the f_σ and b_s particles

at zero temperature according to

$$\begin{aligned}\delta\lambda_f &= \text{Re}\Sigma_f(\lambda_0 + \varepsilon_0 + \delta\lambda_f, T = 0), \\ \delta\lambda_b &= \text{Re}\Sigma_b(\lambda_0 + \delta\lambda_b, T = 0),\end{aligned}\quad (62)$$

note that these real parts diverge linearly with the UV cutoff Λ .

The model (61) shows a transition driven by variation of ε_0 for finite values of V_0 . Tree level scaling analysis shows that

$$\dim[V_0] = \frac{1-r}{2} \equiv \bar{r}. \quad (63)$$

This establishes the role of $r = 1$ as upper-critical dimension where V_0 is marginal.

We now proceed with an RG analysis of (61) which will allow to determine the critical properties for $r \lesssim 1$ – a brief account on this appeared in Ref. 12. The RG will treat the auxiliary fields f_σ and b_s as usual particles and consequently determine their propagator renormalizations, anomalous dimensions etc., but all diagrams are evaluated with $\lambda_0 \rightarrow \infty$ which ensures the non-trivial character of the expansion. Renormalized fields and dimensionless couplings are introduced according to

$$f_\sigma = \sqrt{Z_f} f_{R\sigma}, \quad (64)$$

$$b_s = \sqrt{Z_b} b_R, \quad (65)$$

$$V_0 = \frac{\mu^{\bar{r}} Z_v}{\sqrt{Z_f Z_b}} v. \quad (66)$$

No renormalizations are needed for the bulk fermions as their self-interaction is assumed to be irrelevant in the RG sense.

In contrast to the field theories analyzed in Secs. III A and IV C (where the non-linear coupling is used to tune the system through the phase transition), the theory (61) contains two parameters, namely the tuning parameter ε_0 and the non-linear coupling V_0 . The RG is conveniently performed *at* criticality, i.e., we assume that ε_0 is tuned to the critical line, and RG is done for the coupling v – this naturally results in an infrared stable fixed point. To two-loop order we obtain the following RG beta function:

$$\beta(v) = -\bar{r}v + \frac{3}{2}v^3 + 3v^5 \quad (67)$$

with the calculation given in Appendix C. Generally, the higher-order corrections to the one-loop result appear to be small in the present expansion. One can also consider the flow away from criticality, i.e., the flow of the tuning parameter ε , either using S^2 insertions in the field-theoretic formulation or explicitly within momentum-shell RG. The resulting correlation length exponent is in Eq. (72) below.

The structure of the above RG is very similar to the one of the $(4 - \epsilon)$ expansion of the ϕ^4 model for magnets, where the mass term drives the transition, and the non-linear coupling has a non-trivial stable fixed point at

criticality below four dimensions. Thus, the fixed point with finite v (68) corresponds to the Wilson-Fisher fixed point, whereas $v = 0$ is the analogue of the Gaussian fixed point in the magnetic context, see Fig. 2. The parameters v and ε play the role of the interaction and the mass, respectively.

C. $r^* < r < 1$

For $r < 1$ the trivial fixed point $v^* = 0$ is unstable, and the critical properties are instead controlled by an interacting fixed point at

$$v^{*2} = \frac{2}{3}\bar{r} - \frac{8}{9}\bar{r}^2. \quad (68)$$

At this asymmetric critical fixed point (ACR), we find anomalous field dimensions $\eta_b = 2v^{*2} + 2v^{*4}$, $\eta_f = v^{*2} + 2v^{*4}$. The resulting RG flow diagram is shown in Fig. 2a. The ACR fixed point (Fig. 2b) shifts to larger values of v^{*2} , $|\varepsilon^*|$ with decreasing r , and the expansion can be expected to break down for small r . The numerical results of Ref. 6 show that this is the case at $r^* \approx 0.375$, where ACR merges with SCR, and p-h symmetry is dynamically restored. Then, Eq. (61) together with an expansion in v , \bar{r} yields the correct description of the critical properties for $0.375 \approx r^* < r < 1$. Using NRG we have numerically confirmed this expectation, i.e., the properties of the critical fixed point of the model (61) vary continuously as function of r for $r^* < r < 1$.

D. $r = 1$

For all $r \geq 1$, a phase transition still occurs in the asymmetric Anderson and Kondo models, but it is controlled by the non-interacting VFI fixed point at $v = \varepsilon = 0$. For the marginal case $r = 1$, i.e., at the upper-critical dimension, we expect logarithmic flow. In the following we explicitly keep the UV cutoff Λ , and discuss RG under cutoff reduction $\Lambda \rightarrow \lambda\Lambda$. We restrict ourselves to criticality, where the RG beta function to one-loop order is

$$\beta(v) \equiv \frac{dv}{d \ln \lambda} = \frac{3}{2}v^3 \quad (69)$$

i.e., the hybridization is marginally irrelevant. The RG equation can be integrated to give

$$v^2(\lambda) = \frac{V_0^2}{1 - 3V_0^2 \ln \lambda} \quad (70)$$

with $v(\lambda = 1) = V_0$. This result will be used below to determine logarithmic corrections for a number of observables.

E. $r > 1$

For both exponents $r > 1$ the coupling V_0 in the theory (61) is irrelevant in the RG sense. The critical system flows to the VFI fixed point, Fig. 2b, and the transition becomes a level crossing with perturbative corrections.

Observables can then be obtained by straightforward perturbation theory. Consider, e.g., the boson self-energy (Fig. 14c below):

$$\Sigma_b(i\nu_n) = V_0^2 T \sum_n \int \frac{dk |k|^r}{i\omega_n - k} \frac{1}{i\nu_n - i\omega_n - \lambda_0 - \varepsilon_0},$$

the expression for the fermion self-energy is similar. At the transition, $\varepsilon_0 = 0$, the self-energies show threshold behavior at $T=0$, $-\text{Im} \Sigma_f(\bar{\omega} + i\eta)/\pi \propto V_0^2 \bar{\omega}^r \Theta(\bar{\omega})$ with $\bar{\omega} = \omega - \lambda_0$. The low-energy behavior of the f_σ propagator follows as

$$-\text{Im} G_f(\bar{\omega} + i\eta)/\pi = (1 - A)\delta(\bar{\omega}) + B|\bar{\omega}|^{r-2}\Theta(\bar{\omega}) \quad (71)$$

with $A, B \propto V_0^2$. The b_s propagator has a similar form – we will use these results below to explicitly calculate the local susceptibility.

F. Observables near criticality

We start with the correlation length exponent, ν , of the asymmetric critical fixed point. In the field-theoretic RG scheme it has to be determined via composite operator insertions into the action (61), which take the role of mass terms driving the system away from criticality. The lowest-order result for ν is

$$\frac{1}{\nu} = r + \mathcal{O}(\bar{r}^2) \quad (r < 1), \quad (72)$$

with details of the derivation given in Appendix C. For $r \geq 1$ the transition is a level crossing, formally $\nu = 1$.

In the calculation of observables like susceptibilities etc. the UV behavior depends on whether we are above or below the upper-critical dimension $r = 1$. For $r \geq 1$ the cutoff Λ has to be kept explicitly, as integrals will be UV divergent. This also implies that hyperscaling is violated, and no ω/T scaling in dynamics occurs, as usual for a theory above the upper-critical dimension.

For $r < 1$ the UV cutoff Λ can be sent to infinity after taking into account the contributions of the counter-terms (60), as the remaining integrals are UV convergent. This is in contrast to the expansions for $r \gtrsim 0$ (Sec. III) and for $r \lesssim 1/2$ (Sec. IV), which are effectively both *above* a *lower*-critical dimension, and where intermediate quantities can display UV divergencies. Notably, for all $r < 1$ expansions the low-energy observables are fully universal, i.e., cutoff-independent, and hyperscaling is fulfilled.

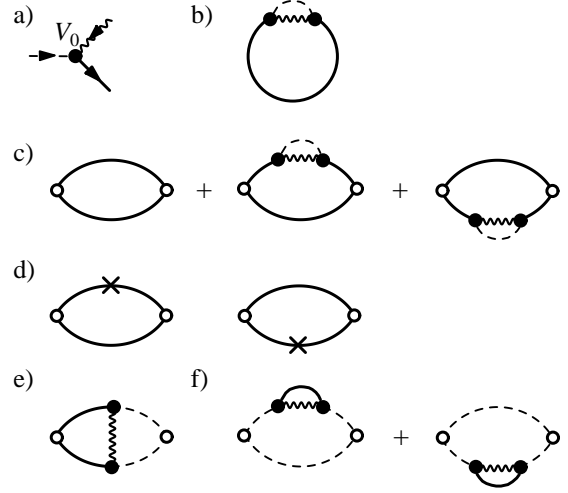


FIG. 8: Feynman diagrams for the infinite- U Anderson model. Full/wiggly/dashed lines denote $f_\sigma/b_s/c_\sigma$ propagators, the cross is the counter-term (60). a) Bare interaction vertex V_0 . b) V_0^2 contribution to the partition function, which also appears in the denominator of Eq. (59). c), d) Diagrams entering the local susceptibility, $\chi_{\text{imp,imp}}$, to order V_0^2 . e) V_0^2 contribution to $\chi_{\text{u,imp}}$. f) V_0^2 contributions to $\chi_{\text{u,u}}$.

1. Local susceptibility

The anomalous exponent η_χ associated with the local susceptibility is calculated as above by determining the χ_{loc} renormalization factor, Z_χ , using minimal subtraction of poles, and then employing

$$\eta_\chi = \beta(v) \left. \frac{d \ln Z_\chi}{dv} \right|_{v^*}. \quad (73)$$

Here we have $\chi_{\text{loc}} = 1/\omega$ at tree level, in contrast to the p-h symmetric problem of Sec. IV.

The leading contributions to Z_χ arise from the diagrams in Fig. 8c, see Appendix C for details. From the Z_χ expression

$$Z_\chi = 1 - \frac{v^2}{\bar{r}} \quad (74)$$

we find η_χ in an expansion in \bar{r} ,

$$\eta_\chi = \frac{2}{3}(1 - r) + \mathcal{O}(\bar{r}^2) \quad (r < 1). \quad (75)$$

This result is again in good agreement with numerical findings⁷, with a comparison given in Fig. 5.

We now describe the evaluation of the logarithmic corrections present at $r = 1$. Using the lowest-order results $\beta(v) = \frac{3}{2}v^3$ and $\eta_\chi(v) = 2v^2$ we can integrate Eq. (73) to yield

$$Z_\chi = \left(\frac{v(\lambda)}{V_0} \right)^{4/3}. \quad (76)$$

The explicit scaling relation³¹ for χ_{loc} at $T = 0$ reads

$$\chi_{\text{loc}}(i\omega, V_0, \Lambda) = Z_\chi (\lambda\Lambda)^{-1} \chi_{\text{loc}} \left(\frac{i\omega}{\lambda\Lambda}, v(\lambda), \Lambda = 1 \right). \quad (77)$$

To analyze the frequency dependence of χ_{loc} we choose $\lambda = \lambda^* = \omega/\Lambda$ and employ (76) together with (70) to express the renormalization factor in terms of λ . This leads to

$$\chi_{\text{loc}}(i\omega, V_0, \Lambda) = \frac{\omega^{-1}}{(1 - 3V_0^2 \ln \frac{\omega}{\Lambda})^{2/3}} \chi_{\text{loc}}(i, v(\lambda), 1).$$

To obtain the leading (i.e. multiplicative) logarithms, the last term can be approximated by its fixed point value, which simply gives a constant – this neglects sub-leading additive logarithmic corrections. We finally obtain the result

$$\chi_{\text{loc}}(\omega) \propto \frac{1}{\omega |\ln \omega|^{2/3}} \quad (r = 1). \quad (78)$$

valid at criticality for $\omega \ll \Lambda$. Note that the structure of the logarithms in our problem is different from e.g. that of the Hertz-Millis theory at the upper-critical dimension studied in Ref. 32. In our problem both v and Z_χ flow to zero according to Eq. (76); whereas in Ref. 32 the renormalization factor Z tends to a non-universal constant as $\lambda \rightarrow 0$ – this leads to the absence of multiplicative logarithms.

Above the upper-critical dimension, $r > 1$, we have simply $\eta_\chi = 0$ and thus $\chi_{\text{loc}} \propto 1/T$ or $\propto 1/\omega$. We shall explicitly demonstrate the calculation of the local impurity susceptibility using bare perturbation theory. To lowest non-trivial order, χ_{loc} is given by the convolution of two f_σ propagators (71), calculated with the self-energy to second order in V_0 . Note that no vertex corrections occur to this order due to the structure of the interaction. When calculating χ_{loc} the $T \rightarrow 0$ limit has to be taken with care, as the exponentially small tail in $\text{Im}G_f(\bar{\omega})$ at $\bar{\omega} < 0$ contributes to χ_{loc} . One obtains for the imaginary part χ''_{loc} for $T \rightarrow 0$ and $1 < r < 2$:

$$\chi''_{\text{loc}}(\omega)/\pi = \frac{1 - 2A}{6} \frac{\delta(\omega)\omega}{T} + \frac{B}{3} |\omega|^{r-2} \text{sgn}(\omega). \quad (79)$$

This shows that ω/T scaling is violated, as the finite frequency part obeys $\chi_{\text{loc}}(\omega \gg T) \propto \omega^{r-2}$, but $\chi_{\text{loc}}(\omega \ll T) \propto T^{-1}$.

Moving away from criticality, one of the f_σ , b_s propagators loses its $\delta(\omega - \lambda_0)$ contribution – for $\varepsilon > 0$ ($t > 0$) this is G_{f_σ} , indicating that free-moment behavior is absent in this regime. Consequently, the zero-temperature static local susceptibility is finite, but diverges upon approaching the critical point according to $\chi_{\text{loc}} \propto t^{r-2}$. For $t < 0$, $\chi_{\text{loc}} \propto 1/T$. Thus, the order parameter m_{loc} jumps at the transition point for $r > 1$.

2. Impurity susceptibility

The evaluation of the impurity susceptibility requires the summation of the diagrams in Fig. 8c–f, appearing in the numerator of the corresponding Eq. (59), and also a careful treatment of the denominator, as we are interested in terms being non-singular as function of \bar{r} .

The diagrams are conveniently evaluated in imaginary time, e.g., the first correction to $\chi_{\text{imp,imp}}$ in Fig. 8c gives

$$\frac{1}{2} e^{-\lambda_0\beta} V_0^2 \int_0^\beta d\tau \int_0^\tau d\tau_2 \int_0^{\tau_2} d\tau_1 G_{c0}(\tau_2 - \tau_1) \quad (80)$$

where the limit $\lambda_0 \rightarrow \infty$ has been taken in the f_σ and b_s propagators. G_{c0} is the conduction electron Green's function at the impurity site, which contains a momentum integral. The other diagrams in Fig. 8 can be written down similarly. Performing the τ integrals first, one obtains

$$\begin{aligned} (8c) &= \frac{1}{T} - V_0^2 \int_0^\Lambda dk \frac{k^r}{k^3} \left[\frac{2k}{T} + \left(4 + \frac{k^2}{T^2} \right) \tanh \frac{k}{2T} \right], \\ (8d) &= -\frac{V_0^2 \Lambda}{T^2}, \\ (8e) &= V_0^2 \int_0^\Lambda dk k^r \frac{2[3 + \cosh(k/T)]k/T - 4 \sinh(k/T)}{k^3 [1 + \cosh(k/T)]}, \\ (8f) &= V_0^2 \int_0^\Lambda dk \frac{k^r}{k^3} \left[4 \tanh \frac{k}{2T} - \left(\frac{2k}{T} + \frac{k^2}{T^2} \tanh \frac{k}{2T} \right) \cosh^{-2} \frac{k}{2T} \right], \quad (81) \end{aligned}$$

where all terms have to be multiplied by $e^{-\lambda_0\beta}/2$. Fig. 8d are the contributions from the counter-terms (60), which evaluate to $\delta\lambda_b = 2\delta\lambda_f = 2V_0^2\Lambda$. The denominator, $\langle \hat{Q} \rangle_{\lambda_0}$, being $3e^{-\lambda_0\beta}$ to zeroth order in V_0 , receives corrections from the diagram in Fig. 8b and from the counter-terms (60), resulting in

$$\langle \hat{Q} \rangle_{\lambda_0} = 3 - 4 \frac{V_0^2 \Lambda}{T} + 4V_0^2 \int_0^\Lambda dk \frac{k^r}{kT} \tanh \frac{k}{2T}, \quad (82)$$

to be multiplied with $e^{-\lambda_0\beta}$. Now we are in the position to collect all contributions to χ_{imp} to second order in V_0 :

$$\begin{aligned} \Delta\chi_{\text{imp}} &= -\frac{V_0^2 T^{-\bar{r}}}{6T} \left[2 \int_0^{\Lambda/T} \frac{dx x^r}{x^3} \frac{\sinh x - x}{1 + \cosh x} \right. \\ &\quad \left. + \int_0^{\Lambda/T} \frac{dx x^r}{3x} \left(\frac{\sinh x}{1 + \cosh x} - 1 \right) \right]. \quad (83) \end{aligned}$$

Note that intermediate terms of the form T^{-2} have cancelled in numerator and denominator of Eq. (59). For $r < 1$ the momentum integrals are UV convergent, and do not develop poles in \bar{r} , i.e., the poles present in the $\chi_{\text{imp,imp}}$ diagrams have been cancelled by contributions from Fig. 8e/f. In the low-energy limit, the product

$V_0^2 T^{-\bar{r}}$ approaches a universal value. Thus χ_{imp} has indeed Curie form, with a fully universal prefactor depending on r only. For $r > 1$ the integrals require an explicit UV cutoff, but no correction to the Curie term arises, as $(V_0^2 T^{-\bar{r}})$ vanishes as $T \rightarrow 0$.

Performing the integral for $r < 1$ and expressing the result in terms of the renormalized coupling v , the impurity susceptibility reads

$$T\chi_{\text{imp}} = \frac{1}{6} - \left(\frac{1}{6} - \frac{\ln 2}{9}\right)v^2 + \mathcal{O}(v^4) \quad (84)$$

With the value of the coupling at the ACR fixed point (68) we finally find, to leading order in $(1-r)$,

$$T\chi_{\text{imp}} = \begin{cases} \frac{1}{6} - 0.02988(1-r) + \mathcal{O}(\bar{r}^2) & (r < 1) \\ \frac{1}{6} & (r \geq 1) \end{cases}, \quad (85)$$

to be compared with the numerical results in Fig. 6.

3. Impurity entropy

The impurity contribution to the entropy can be derived from the free energy as above. At the VFI fixed point the entropy is $S_{\text{imp}} = \ln 3$, and the lowest-order correction is computed by expanding the free energy in v . Note that this correction vanishes for $r \geq 1$, as $v^* = 0$ there.

The calculation of the impurity entropy in the presence of a constraint for pseudoparticles has been discussed in Appendix C of Ref. 26. The limit $\lambda_0 \rightarrow \infty$ suppresses all contributions from the unphysical part of the Hilbert space, in particular disconnected diagrams in the partition function. Remarkably, this leads to the appearance of disconnected diagrams in higher-order terms of the expansion for the thermodynamic potential Ω . The second-order diagram for Ω , shown in Fig. 8b, evaluates to

$$\Delta\Omega_{\text{imp}} = \frac{2V_0^2}{3} \int_{-\Lambda}^{\Lambda} dk \frac{|k|^r}{k} \tanh \frac{k}{2T}. \quad (86)$$

There is also a contribution to Ω_{imp} from the counterterms, but this is temperature-independent and does not contribute to the entropy. Taking the temperature derivative we find:

$$\Delta S_{\text{imp}} = -\frac{V_0^2}{3} T^{-2\bar{r}} \int_{-\Lambda/T}^{\Lambda/T} dx |x|^r \cosh^{-2} \frac{x}{2}. \quad (87)$$

This integral can be performed in the limit of infinite UV cutoff. [In contrast, the integral in (86) is UV divergent, as discussed in Sec. II.] Expressing the result in terms of the renormalized hybridization and taking the limit $r \rightarrow 1$ we have

$$S_{\text{imp}} = \ln 3 - \frac{8 \ln 2}{3} v^2. \quad (88)$$

As expected, the entropy correction is fully universal and finite in the limit $T \rightarrow 0$. Inserting the fixed point value of the coupling v into Eq. (88), we find the impurity entropy as

$$S_{\text{imp}} = \begin{cases} \ln 3 - \frac{8 \ln 2}{9}(1-r) + \mathcal{O}(\bar{r}^2) & (r < 1) \\ \ln 3 & (r \geq 1) \end{cases}. \quad (89)$$

NRG calculations⁶ have determined S_{imp} for r values below unity; a comparison is shown in Fig. 7. As with most of the observables obtained within the $(1-r)$ expansion the agreement of the lowest-order result with numerics is surprisingly good even for r values well away from unity, indicating that higher-loop corrections are small.

The results for the RG flow and the impurity entropy have an interesting corollary: Stability analysis shows that for $r^* < r < \frac{1}{2}$ the RG flow at criticality and small p-h asymmetry is from SCR to ACR. The entropy of SCR approaches $\ln 2$ as $r \rightarrow \frac{1}{2}$. Both NRG and the above expansion indicate that the entropy of ACR is *larger* than $\ln 2$ for $r \lesssim \frac{1}{2}$, Fig. 7. Thus we have $S_{\text{imp,ACR}} > S_{\text{imp,SCR}}$ for $r^* < r < \frac{1}{2}$, i.e., the impurity part of the entropy increases under RG flow (see also Fig. 9 below), in contradiction to the so-called g -theorem²¹! (This is not a fundamental problem, as the present model has effectively long-ranged interactions, and is not conformally invariant, such that the proof of the g -theorem does not apply.)

4. Conduction electron T matrix

The T matrix in the Anderson model is given by $T(\omega) = V_0^2 G_f(\omega)$. The physical f propagator G_f is a convolution of the auxiliary f_σ and b_s propagators, i.e., the propagator of the composite operator $(f_\sigma^\dagger b_s)$. The anomalous exponent is obtained from

$$\eta_T = \beta(v) \left. \frac{d \ln Z_T}{dv} \right|_{v^*}. \quad (90)$$

As in Ref. 28 we are able to determine an *exact* result for the anomalous exponent, valid to all orders in perturbation theory. The argument is based on the diagrammatic structure of the T matrix, namely the relevant diagrams can be completely constructed from full v interaction vertices and full f/b propagators²⁸. This leads to the relation between Z factors

$$Z_T^{-1} = \frac{Z_v^2}{Z_f Z_b}. \quad (91)$$

This equation can be plugged into (66). Taking the logarithmic derivative at fixed bare coupling and using $\beta(v)/v = 0$ at any fixed point with finite v^* , one obtains the exact result

$$\eta_T = 2\bar{r} \quad \Rightarrow \quad \text{Im}T(\omega) \propto |\omega|^{-r}. \quad (92)$$

Whereas Eq. (92) applies to the p-h asymmetric fixed point (ACR), and is valid for $r^* < r < 1$, the results of

Sec. IV H and Ref. 28 have established the same critical behavior for the T matrix for the symmetric fixed point (SCR) for $0 < r < \frac{1}{2}$. Thus, we conclude that all critical fixed points for $0 < r < 1$ in the pseudogap Anderson and Kondo models display a T matrix behavior of $\text{Im}T(\omega) \propto |\omega|^{-r}$.

The logarithmic correction to the T matrix at $r = 1$ are evaluated in a manner similar to the one for the local susceptibility above. With $\beta(v) = \frac{3}{2}v^3$ and $\eta_T(v) = 3v^2$ – note that $\eta_T = \eta_f + \eta_b$ only holds at one-loop level because $Z_v = 1$ at this order – we can integrate (90) to find

$$Z_T = \left(\frac{v(\lambda)}{V_0} \right)^2. \quad (93)$$

With the general scaling relation

$$T(i\omega, V_0, \Lambda) = Z_T (\lambda\Lambda)^{-1} T\left(\frac{i\omega}{\lambda\Lambda}, v(\lambda), \Lambda = 1\right) \quad (94)$$

and (70) we find

$$T(i\omega, V_0, \Lambda) = \frac{\omega^{-1}}{1 - 3V_0^2 \ln \frac{\omega}{\Lambda}} T(i, v(\lambda), 1).$$

As above, the leading logarithms are of multiplicative character, with the final result $T(\omega) \propto 1/(\omega |\ln \omega|)$. This implies for the T matrix spectral density the behavior

$$\text{Im}T(\omega) \propto \frac{1}{\omega |\ln \omega|^2} \quad (r = 1). \quad (95)$$

Above the upper-critical dimension, $r > 1$, we have again $\eta_T = 0$ and $\text{Im}T(\omega) \propto \delta(\omega)$.

VI. GENERAL PARTICLE-HOLE ASYMMETRY

Here we comment on the general case of finite p-h asymmetry. Starting with the trivial fixed points, tree-level power counting shows that LM is stable w.r.t. p-h asymmetry, with a scaling dimension of $-r$. In contrast, SSC is unstable towards ASC, and p-h asymmetry grows near SSC with a scaling dimension of r . Finally, at the free-impurity fixed point (FImp) p-h asymmetry grows under RG with a scaling dimension of unity and the systems flow towards VF1. VF1 itself is stable w.r.t. a deviation from maximal p-h asymmetry.

In the r ranges where the RG expansions of this paper are perturbatively controlled, we can immediately come to conclusions about the stability of the critical fixed points: SCR will be stable w.r.t. finite p-h asymmetry for r close to 0, but unstable for r close to $\frac{1}{2}$. Similarly, for r close to or larger than unity, ACR is stable w.r.t. a deviation from maximal p-h asymmetry, in other words it is safe to discard one of the two impurity states, $|d\rangle$ or $|e\rangle$, for the discussion of the critical properties, and to work with the perturbative expansion of Sec. V. One has to

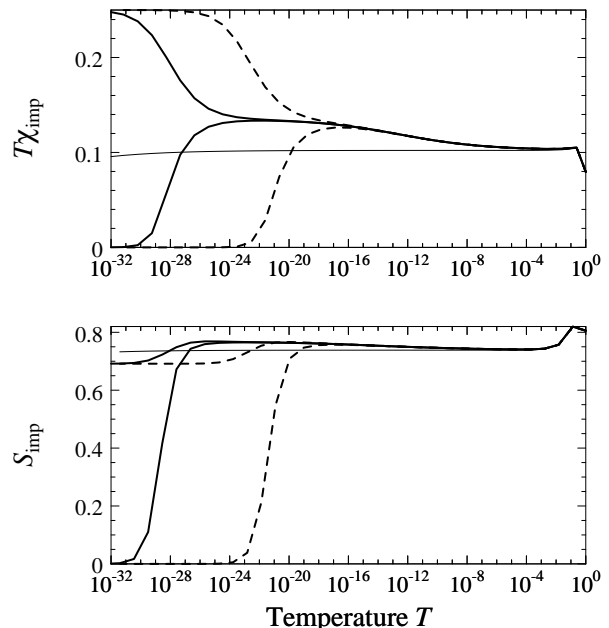


FIG. 9: NRG results for a slightly p-h asymmetric Anderson model at $r = 0.45$ close to criticality (ACR). Parameter values are a hybridization strength $\pi V_0^2 \rho(0) = 1$, $\varepsilon_0 = -0.5$, and $U_0 = 0.9949, 0.99493, 0.9949213, 0.9949215$ (solid). The thin lines are for a p-h symmetric model very close to criticality (SCR), with $\varepsilon_0 = -0.487$, $U_0 = 0.974$. The NRG runs were done using a discretization parameter of $\Lambda = 9$, keeping $N_s = 650$ levels. The two-stage flow described in the text can be clearly seen, i.e., there is a small energy scale T^* where the system flows from ACR to ASC or LM (solid: $T^* \approx 10^{-28}$, dashed: $T^* \approx 10^{-22}$), and a larger scale $T_{\text{ACR}} \approx 10^{-12}$ where the system flows from SCR to ACR. a) Impurity susceptibility $T\chi_{\text{imp}}$. b) Impurity entropy S_{imp} . The behavior of the entropy illustrates the point made in Sec. V F 3: $S_{\text{imp}}(T)$ decreases as function of T , i.e., *increases* along the RG flow, for $T^* < T < T_{\text{ACR}}$ due to $S_{\text{imp,ACR}} > S_{\text{imp,SCR}}$. This “uphill flow” does not violate thermodynamic stability criteria, as the total entropy (impurity plus bath) of the system still decreases under RG.

keep in mind that ACR moves towards smaller effective p-h asymmetry (larger values of $|\varepsilon^*|$) upon decreasing r , and the perturbative expansion around VF1 breaks down as $r \rightarrow r^{*+}$ where p-h symmetry is dynamically restored.

The numerics of Ref. 6 gives no indications for additional fixed points in the case of finite p-h asymmetry which would not be present in the maximally asymmetric model; our RG results are consistent with this. Thus, the critical properties of a pseudogap Kondo or Anderson model with general p-h asymmetry are always identical to the ones of the maximally asymmetric model of Sec. V.

For the RG treatment of a model with general p-h asymmetry close to criticality one has to envision a *two-step* RG procedure, as usual in problems with different energy scales. Suppose we start near criticality from small hybridization and small p-h asymmetry. For $r > r^*$, the scaling dimension of p-h symmetry breaking

term is largest: at tree level we have $\dim[2\varepsilon_0 + U_0] = 1$ and $\dim[V_0] = (1 - r)/2$. Thus the initial model parameters flow towards large p-h asymmetry first. This flow drives the system into the regime described by the maximally p-h asymmetric Anderson model of Sec. V, thereby renormalizing the parameters ε and v . Then, the RG of Sec. V takes over, with a flow towards ACR, and finally to one of the two stable phases (if the system is not exactly at criticality). Thus, a low-energy scale T^* and a higher scale T_{ACR} exist, where T_{ACR} characterizes the approach of the effective p-h asymmetry towards the ACR fixed point. Note that for $r > 2$ the fastest flow is the one of v to zero, i.e., the system quickly approaches the VFL fixed point. The described behavior is nicely borne out by NRG calculations for the Anderson model, see Fig. 9.

Finally, for $r < r^*$ the initial flow is dominated by the decrease of p-h asymmetry – this cannot be captured by our Anderson model RG, but is contained in the Kondo treatment – and the system approaches SCR, before it finally departs to one of the two stable phases. If the system is on the strong-coupling side of the transition ($t > 0$), then the behavior near SCR is multicritical (see also Fig. 16a of Ref. 6): two low-energy scales exist which describe the departure of the flow from SCR, namely T^* (for the deviation of j from j^*) and a *lower* scale T_{ASC} (for the subsequent growth of p-h asymmetry when flowing towards the ASC fixed point).

We note that a recent investigation of the pseudogap Anderson model³³ using the local-moment approach⁸ has found indications of a line of critical fixed points in the p-h asymmetric case, parametrized by p-h asymmetry. We believe that this is an artifact of the employed approximation scheme, as (i) NRG calculations strongly hint towards a single asymmetric critical fixed point (for fixed r), i.e., the fixed-point level spectrum at criticality does not depend on the initial p-h asymmetry (e.g. the ratio U_0/ε_0), and (ii) our analytical RG shows that, at least near $r = 1$, the scaling dimension of p-h asymmetry is largest, and the sketched two-step RG (which directly leads to consider an infinite- U Anderson model to describe the critical behavior) is a controlled approach for arbitrary initial p-h asymmetry.

VII. RELATION BETWEEN ANDERSON AND KONDO MODELS

This section shall highlight the relation between the pseudogap Anderson and Kondo impurity models.

On the one hand, it is well-known that the Anderson model reduces to the Kondo model in the so-called Kondo limit, see Sec. IA. This mapping covers the far left-hand side of the flow diagrams in Figs. 1 and 2, and suggests that the phase transition at small r in the Anderson model in this Kondo limit is described by the Kondo RG of Sec. III.

On the other hand, we have argued that the flow of the Kondo model can be naturally understood in terms

of the variables of the Anderson model. In particular, the RG expansions of Secs. IV and V, describing transitions of the Anderson model near $r = \frac{1}{2}$ and $r = 1$, also apply to the Kondo model. Clearly, in thinking about this “mapping” of the Kondo to the Anderson model one has to view the Anderson model as an effective *low-energy* theory of the Kondo model. The impurity states of this effective Anderson model are thus many-body states obtained after integrating out high-energy degrees of freedom from the Kondo model, i.e., dressed impurity states.

A formal way to obtain an Anderson model from a Kondo model is a strong-coupling expansion: The $|\uparrow\rangle$ and $|\downarrow\rangle$ states of the Anderson model are bare impurity states, whereas $|e\rangle$ and $|d\rangle$ represent the impurity with either a hole or an electron of opposite spin tightly bound to the impurity.

The above can also be made plausible in a slightly different way, in the following for a p-h asymmetric situation: Let us consider the Kondo problem with a hard-gap DOS³⁴: in the presence of p-h asymmetry it shows a first-order quantum transition, i.e., a level crossing, between a Kondo-screened singlet and a spin- $\frac{1}{2}$ doublet state. As we can understand the asymmetric pseudogap DOS as consisting of an asymmetric high-energy part and a (asymptotically) symmetric low-energy part, we can obtain an effective theory for the pseudogap Kondo model by coupling the above mentioned three (many-body) impurity states, obtained by integrating out high-energy degrees of freedom from the band, to the remaining low-energy part of the conduction electron spectrum. A crucial ingredient is now the p-h asymmetry of the original model. It is clear that upon integrating out the high-energy part of the bath *two* many-body singlet states arise, namely $|e\rangle$ and $|d\rangle$ as discussed above. Due to the p-h asymmetry of the underlying model these two singlet states will have very different energies, such that we can discard the high-energy state in the low-energy theory. With this we directly arrive at an infinite- U pseudogap Anderson model.

We conclude that the phase transitions of the pseudogap Anderson and Kondo models are in the same universality classes – this is supported by the numerical calculations of Ref. 6. For small r the phase transition is naturally described in the Kondo language of Sec. III, implying that the critical fixed point of the Anderson model is located in the Kondo limit. In contrast, for larger r the formulation in terms of the Anderson model provides the relevant degrees of freedom, in other words, both spinful and spinless (many-body) impurity states play a role in the critical dynamics.

VIII. FINITE MAGNETIC FIELD

Interesting physics obtains in the pseudogap Kondo and Anderson models in the presence of a finite magnetic field. We concentrate here on the effect of a *local* field, applied to the impurity only. Note that a finite field

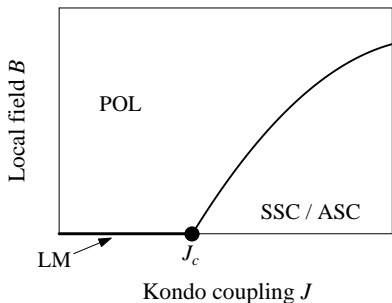


FIG. 10: Schematic $T = 0$ phase diagram of the pseudogap Kondo model in a local magnetic field B . At $B = 0$, there is a phase transition at $J_K = J_c$ between LM and a strong-coupling phase, SSC or ASC. Upon application of a field, an unscreened spin becomes strongly polarized (POL), whereas a screened spin in a strong-coupling phase is only weakly polarized. Increasing the field at $J_K > J_c$ drives a phase transition – such a transition is *not* present in the metallic case, $r = 0$. The phase diagram for a pseudogap Anderson model is similar. As discussed in the text, the zero-field critical fixed point is always unstable w.r.t. finite B in the RG sense; thus the two transitions are in general in different universality classes (which is already clear from symmetry considerations).

applied to the bulk can modify the low-energy behavior of the bath DOS due to Zeeman splitting; then, pseudogap Kondo physics survives only for energy scales above the Zeeman energy.

For $T = 0$ and a metallic density of states, $r = 0$, a local field B only leads to a crossover as function of B/T_K , and all observables evolve smoothly from $B = 0$ (screened spin) to large B (polarized spin). In contrast, for any $r > 0$ and $t > 0$ (i.e. $J_K > J_c$ in the Kondo model) there will be a zero-temperature phase transition as function of the local field between one phase with weak and one with strong impurity spin polarization, see Fig. 10. We briefly discuss this phase transition in the following – it turns out that the variables of the Anderson model provide a natural language to analyze the problem. Remarkably, all ingredients needed for the discussion of the critical properties have already been calculated in the previous sections.

Strategically, we first discuss the decoupled impurity, and then analyze the modifications arising from the presence of the hybridization term. For the decoupled impurity, the local field is trivially a relevant perturbation, with scaling dimension unity. Thus, in the low-energy limit the field is effectively infinite, and one of the two impurity states $|\uparrow\rangle$, $|\downarrow\rangle$ can be discarded (we will discard $|\downarrow\rangle$ in what follows).

A. Asymmetric Anderson model

In the p-h asymmetric case two impurity states have to be considered, namely $|\uparrow\rangle$ and $|e\rangle$. We discuss a level

crossing transition of these two, tunable e.g. by varying the magnetic field, and being coupled to conduction electrons. At the transition we are left with a (spinless) resonant level model, and the analysis for a pseudogap host density of states is in Sec. IV B. In particular, for $r > 1$ the phase transition is a level crossing with perturbative corrections, and for all $0 < r < 1$ we have a continuous transition with a critical fixed point identical to the intermediate-coupling fixed point of the resonant level model, Eq. (31). Thus, the properties of the transition evolve smoothly as function of r for $0 < r < 1$, in contrast to the zero-field situation (!).

B. Symmetric Anderson model

In the presence of p-h symmetry and magnetic field, the decoupled impurity has three low-energy states: $|\uparrow\rangle$, $|e\rangle$, $|d\rangle$. The resulting level-crossing transition is technically identical to the one of the zero-field infinite- U Anderson model of Sec. V: the two situations can be mapped onto each other via the p-h transformation (3). From Sec. V we can read off the properties of the field-tuned phase transition: For $r > 1$ we have again a level crossing with perturbative corrections. A RG expansion around the level-crossing fixed point can be used to calculate the critical properties below $r = 1$. This expansion describes the physics for all $r > r^*$.

It is interesting to ask what happens for $r < r^*$. At r^* the broken level symmetry is dynamically restored at the critical fixed point, meaning that for $r < r^*$ the transition is controlled by a zero-field critical fixed point. From Secs. III and IV we know that for $r < \frac{1}{2}$ such an Anderson model transition with four degenerate impurity states is the same as described by the weak-coupling RG in the Kondo language. However, the mapping (3) shows that we have to consider a Kondo model of a charge pseudospin here, i.e., the corresponding Schrieffer-Wolff transformation will project out the $|\uparrow\rangle$ and $|\downarrow\rangle$ states. In other words, in a p-h symmetric situation with $0 < r < r^*$, where the zero-field transition is controlled by the SCR fixed point, the finite-field transition will be asymptotically controlled by the SCR' fixed point!

C. Kondo model

The above statement is consistent with a simple generalization of the weak-coupling RG of Sec. III to the case of finite field. One easily finds that the field is a relevant perturbation at the SCR fixed point with a scaling dimension of unity, and the finite-field transition is *not* accessible in a description using the Kondo model spin variables. (In contrast, the magnetic field is irrelevant at SCR'.)

D. Symmetries and pseudospin field

In the Anderson model language, the local field lifts the degeneracy of the magnetic doublet $|\uparrow\rangle, |\downarrow\rangle$. It breaks the SU(2) symmetry in the spin sector, and the effect is clearly independent of the field direction.

As discussed in Sec. IA, the p-h symmetric Anderson model display SU(2) symmetry also in the charge sector (charge pseudospin). This can be broken by choosing $U_0 \neq -2\varepsilon_0$, corresponding to a pseudospin field in z direction. Clearly, a pseudospin field in perpendicular direction will have the same effect – this field corresponds to a local pairing field coupling to $f_\uparrow f_\downarrow$. Thus, the SU(2) pseudospin symmetry shows that the effect of s -wave pairing correlations on the Kondo problem is similar to a particle-hole asymmetry, as argued in Ref. 35 using a completely different approach.

IX. CONCLUSIONS

In this paper, we have analyzed the zero-temperature phase transitions in the pseudogap Kondo problem, characterized by a bath density of states $\rho(\omega) \propto |\omega|^r$. Using various perturbative RG expansions, formulated in the degrees of freedom of either the Kondo or the Anderson impurity model, we have developed critical theories for the phase transitions in both the p-h symmetric and asymmetric cases. We have established that $r = 0$ and $r = \frac{1}{2}$ play the role of two lower-critical dimensions in the p-h symmetric case, i.e., the non-trivial phase transition disappears both as $r \rightarrow 0^+$ and $r \rightarrow \frac{1}{2}^-$ with diverging correlation length exponent. In contrast, $r = 1$ is an upper-critical dimension for the p-h asymmetric model. The transitions for $0 < r < 1$ are described by interacting field theories with *universal* local-moment fluctuations and strong hyperscaling properties including ω/T scaling of dynamical quantities. In contrast, for $r > 1$ we find a level crossing with perturbative corrections, and hyperscaling is violated.

In the p-h symmetric case, we found two different expansions, one around $r = 0$ and one around $r = \frac{1}{2}$, to describe the same critical fixed point. In the presence of p-h asymmetry, a different critical fixed point emerges, which can be analyzed in an expansion around $r = 1$.

Apart from the small- r expansion of Sec. III, all our theories were formulated using the Anderson model language. This shows that the quantum phase transition between a screened and an unscreened moment in Kondo-type models can be nicely interpreted by saying that the system fluctuates between “possessing a moment” and “possessing no moment” – this is precisely what is described by the effective Anderson model at its valence-fluctuation fixed point.

We have calculated a number of observables, with results being in excellent agreement with numerical data. In particular, we have found an exact exponent for the conduction electron T matrix, valid for all expansions

used in this paper. We have also discussed the physics of the pseudogap Kondo problem in a local magnetic field, where we have shown that – in contrast to the metallic Kondo effect – a sharp transition occurs as a function of the field.

Applications of our results include impurity moments in unconventional superconductors^{9,10,23,25} and other pseudogap systems, like e.g. graphite. On the theoretical side, we expect that the analysis of quantum impurity models using Anderson instead of Kondo model variables may be useful in a variety of problems. Thus, field theories similar to ours can possibly be constructed for other impurity quantum transitions, and will also be useful for the study of lattice models in dynamical mean-field theory³⁶ and its extensions³⁷, where local quantum criticality can be captured using effective single-impurity models.

Acknowledgments

We thank L. Balents, R. Bulla, M. P. A. Fisher, S. Florens, M. Kir an, K. Ingersent, N. Read, A. Rosch, Q. Si, P. W olfl e and in particular S. Sachdev for illuminating discussions, and R. Bulla and T. Pruschke for help with the NRG calculations. This research was supported by the Deutsche Forschungsgemeinschaft through the Center for Functional Nanostructures Karlsruhe. MV also acknowledges support by the National Science Foundation under Grant No. PHY99-0794 and the hospitality of KITP Santa Barbara where part of this work was carried out.

APPENDIX A: THE NON-INTERACTING RESONANT LEVEL MODEL

Here we provide a few details about the non-interacting resonant level model with a pseudogap density of states. The model is exactly solvable, and all properties can be directly evaluated using the dressed f electron propagator (26). The local susceptibility has been quoted in Sec. IV B. The T matrix is given by $T(\omega) = V_0^2 G_f(\omega)$; a brief discussion of spectral properties can also be found in the Appendix of Ref. 6.

We now sketch the calculation of $T\chi_{\text{imp}}$ and S_{imp} . The diagrams contributing to $T\chi_{\text{imp}}$ are in Fig. 11; note that these contain full f propagators, and no higher-order diagrams appear. Power counting shows that terms of $1/T$ form do only arise from $\chi_{\text{u,u}}$; both $\chi_{\text{imp,imp}}$ and $\chi_{\text{u,imp}}$ are less singular. The evaluation of the diagrams in Fig. 11c gives

$$\begin{aligned} \chi_{\text{u,u}}(T) &= \frac{V_0^2}{A_0} T \sum_n \int_{-\Lambda}^{\Lambda} dk |k|^r \frac{|\omega_n|^{-r}}{(i\omega_n - k)^3} \quad (\text{A1}) \\ &+ \frac{V_0^4}{2A_0^2} T \sum_n \left(\int_{-\Lambda}^{\Lambda} dk |k|^r \frac{|\omega_n|^{-r}}{(i\omega_n - k)^2} \right)^2. \end{aligned}$$

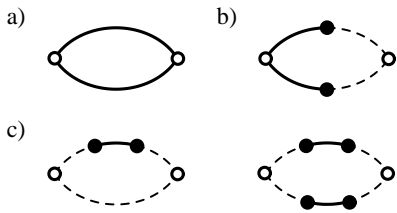


FIG. 11: Feynman diagrams for the spin susceptibility of the non-interacting resonant level model of Sec. IV B. Dashed/full lines denote c_σ /dressed f_σ propagators, respectively; the full dots are V_0 vertices, and the open circles are sources. a) $\chi_{\text{imp,imp}}$. b) $\chi_{\text{u,imp}}$. c) $\chi_{\text{u,u}}$. Note that the displayed diagrams give the *exact* results for the susceptibilities, as all self-energies are contained in the dressed f propagator.

All factors of V_0 cancel exactly against the A_0 , and we obtain a quantity with a universal prefactor. The k integrals can be performed in the limit of infinite UV cutoff, followed by the Matsubara summations. The result is of Curie form, with

$$\chi_{\text{u,u}}(T) = \frac{r}{8T}. \quad (\text{A2})$$

Note that we have used the dressed f propagators (26) in their low-energy form – due to their singular nature their high-energy properties are unimportant for the leading low-temperature behavior of the susceptibility.

The impurity entropy S_{imp} is directly calculated from the full f propagator (26). Performing the $\text{tr} \ln$ in the partition function gives

$$\Omega_{\text{imp}} = -2T \sum_n \ln[i \text{sgn}(\omega_n) |\omega_n|^r]. \quad (\text{A3})$$

One can easily see that the $T = 0$ entropy contributions of $\ln(i\omega_n)$ and $\ln|\omega_n|$ are identical, thus we have

$$S_{\text{imp}} = - \lim_{T \rightarrow 0} \partial_T \left(-2rT \sum_n \ln(i\omega_n) e^{i\omega_n 0^+} \right). \quad (\text{A4})$$

This is nothing but $2r$ times the entropy of a free spinless fermion, resulting in $S_{\text{imp}} = 2r \ln 2$.

Interestingly, the above exact universal results can also be obtained in the framework of a RG expansion in the hybridization, i.e., in a formal expansion around $r = 1$. Here one exploits the intermediate-coupling nature of the fixed point, by calculating observables using renormalized perturbation theory and employing the fixed-point value (31) of the coupling v . The necessary diagrams, Fig. 12, now contain *bare* (instead of dressed) f propagators. Technically, higher-order terms appear in this expansion, but upon interpreting the lowest-order result of renormalized perturbation theory (e.g. re-exponentiating logarithms) these terms are completely summed up. Thus, within the RG framework the information about the non-trivial f scaling dimension is

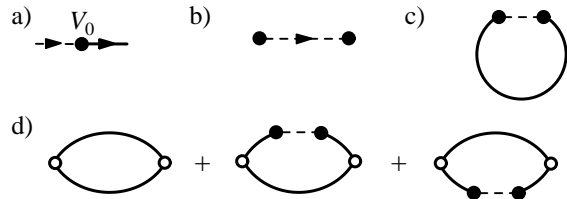


FIG. 12: Diagrams occurring in the perturbative RG for the non-interacting resonant level model of Sec. IV B. Here, full lines are *bare* f_σ propagators. a) Bare interaction vertex V_0 . b) f_σ self-energy. c) Diagram for the v^2 entropy correction. d) Diagrams entering the local susceptibility to order v^2 . Within the renormalized perturbation theory scheme all corrections beyond second order in v vanish.

contained in the coupling value v^* instead of in the propagator G_f . We briefly demonstrate the idea by evaluating the impurity entropy. As we expand around $v = 0$ (the FImp fixed point) we obtain a perturbative correction to the impurity thermodynamic potential which is of order V_0^2 (Fig. 12b). Taking the temperature derivative leads to

$$\Delta S_{\text{imp}} = -\frac{V_0^2}{2} T^{-2\bar{r}} \int_{-\Lambda/T}^{\Lambda/T} dx |x|^r \cosh^{-2} \frac{x}{2} \quad (\text{A5})$$

with $\bar{r} = (1 - r)/2$ as above. Performing the integral in the limits $\Lambda \rightarrow \infty$ and $r \rightarrow 1$ and introducing the renormalized hybridization v yields

$$S_{\text{imp}} = (1 - 2v^2) \ln 4. \quad (\text{A6})$$

With the fixed point value of the hybridization we obtain the result $S_{\text{imp}} = 2r \ln 2$ as above.

APPENDIX B: RG FOR THE INTERACTING RESONANT-LEVEL MODEL

In this appendix we present details of the renormalization group treatment for the symmetric Anderson model in the vicinity of $r = \frac{1}{2}$. It is based on an expansion around the SSC fixed point, i.e., around a non-interacting resonant-level model, with the interaction strength being the expansion parameter. Thus the expansion is done around an intermediate-coupling fixed point (!).

The starting point is the action (36) derived in Sec. IV C, for $0 < r < 1$. Importantly, the “bare” (i.e. $U_0 = 0$) f propagator in (36) behaves as $1/(A_0 \omega^r)$ at low energies, Eq. (26), as the conduction electrons have already been integrated out. The prefactor A_0 will be kept explicitly in the renormalization steps. We employ the field-theoretic RG scheme in order to determine the flow of the coupling renormalized coupling u , introduced in Eq. (39), with dimensional regularization and minimal subtraction of poles. As will be seen below, the lowest non-trivial renormalizations arise at two-loop order.

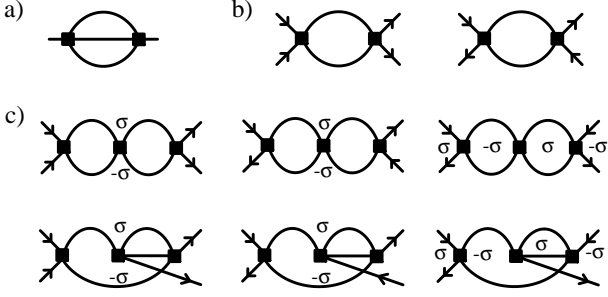


FIG. 13: Diagrams for the RG of the symmetric Anderson impurity model, with notation as in Fig. 4. a) U_0^2 self-energy contribution, which vanishes. b) One-loop vertex renormalizations, which vanish due to p-h symmetry. c) Two-loop vertex renormalizations – these are the only contributions to the beta function (41).

The needed diagrams arising in the RG treatment are displayed in Fig. 13. A number of observations can be made: (i) Hartree diagrams vanish due to the overall p-h symmetry of the model. (ii) Explicit calculation shows that the one-loop vertex renormalization diagrams, i.e., the u^2 corrections to u in Fig. 13b, do not develop ϵ poles. This also follows from the fact that the beta function cannot contain even powers in u due to p-h symmetry. (iii) Explicit evaluation shows that the f self-energy up to two-loop order, Fig. 13a, does not contribute singular propagator renormalizations. In other words, the field renormalization factor is

$$Z = 1 \quad (\text{B1})$$

to two-loop order. As we will argue below, this result is *exact* to all orders in perturbation theory. It implies that the f field does not acquire an anomalous dimension, $\eta_f = 0$.

The two-loop diagrams for the renormalization of u can be divided into two groups of three each, displayed in the two lines of Figs. 13c. The diagrams in each group can be easily seen to be equal. Explicitly:

$$(13\text{c1}) = U_0^3 \left[\int \frac{d\omega_1}{2\pi} G_f(i\omega_1) G_f(i\omega_1 + i\nu) \right]^2 \quad (\text{B2})$$

where ν is the sum of two external frequencies. Using the explicit form of G_f (26), the frequency integral can be split according to the absolute value in G_f , and then performed directly with UV cutoff sent to infinity. The result contains ϵ poles and reads

$$(13\text{c1}) = U_0^3 \frac{\nu^{2-4r}}{\pi^2} \left[\frac{1}{\epsilon^2} + \frac{\pi - 2 \ln 4}{\epsilon} + \mathcal{O}(\epsilon^0) \right]. \quad (\text{B3})$$

The second group of diagrams in Fig. 13c is slightly more complicated. All three of them can be brought into the form

$$(13\text{c4}) = 2U_0^3 \int \frac{d\omega_1}{2\pi} \frac{d\omega_2}{2\pi} G_f(i\omega_1) G_f(\omega_2) \times G_f(-i\omega_1 + i\nu) G_f(i\omega_2 - i\omega_1 + i\nu) \quad (\text{B4})$$

where the prefactor 2 accounts for the different arrangement of the vertices, and ω is a (third) external frequency. The ω_2 integral can be performed directly and leads to the same expression that occurred in the brackets in (B2). The remaining ω_1 integral can also be performed after splitting the interval into four parts. Straightforward algebra, using the identity $\arcsin \sqrt{x} - i \operatorname{arctanh} \sqrt{1-1/x} = \pi/2$, where $x = \omega/\nu < 1$, leads to

$$(13\text{c4}) = U_0^3 \frac{\nu^{2-4r}}{\pi^2} \left[-\frac{1}{\epsilon^2} - \frac{3(\pi - 2 \ln 4)}{2\epsilon} + \mathcal{O}(\epsilon^0) \right]. \quad (\text{B5})$$

Upon adding the contributions from 13c1–13c6, only single poles in ϵ remain – as $Z = 1$, the cancellation of the double poles is a consistency check of our calculation. Minimal subtraction of poles at external frequencies set to μ yields the renormalization factor for the quartic coupling:

$$Z_4 = 1 + \frac{3(\pi - 2 \ln 4)u^2}{2\pi^2\epsilon}. \quad (\text{B6})$$

The RG beta function can be evaluated by taking the μ derivatives of (39) at fixed bare coupling,

$$\beta(u) \equiv \mu \frac{du}{d\mu} \Big|_{U_0} = \epsilon u \left(1 - \frac{3(\pi - 2 \ln 4)u^2}{\pi^2 \epsilon} \right), \quad (\text{B7})$$

which is the result in Eq. (41).

We now provide the proof for $Z = 1$, i.e., no singular propagator renormalizations occur in the present problem. What is needed is p-h symmetry and the form of the bare propagator, $G_f \propto \omega^{-1/2}$ or $G_f(\tau) \propto \tau^{-1/2}$ in the low-energy limit for $r = \frac{1}{2}$. We argue that no logarithms arise when evaluating the self-energy at $r = \frac{1}{2}$. By power counting, all f self-energy diagrams in the τ domain give a result proportional to $\tau^{-3/2}$. Let us discuss internal τ integrals arising in the evaluation (which could produce logs). In the first step, those involve four G_f propagators due to the quartic interaction – here it is important that tadpoles do not contribute due to p-h symmetry. Therefore, the integrand will behave as τ^{-2} , and logs cannot occur. In further steps, four propagators do not necessarily occur, but the power counting argument shows that each internal time still has to occur with a power of τ^{-2} . This shows that the integrands will always be *more singular* than $1/\tau$, and no logarithms arise. Clearly, such an argument cannot be constructed for the vertex diagrams, as they behave as $1/\tau$ at $r = \frac{1}{2}$, and Fourier transformation generically yields an ϵ pole.

Let us turn to the local susceptibility renormalization factor Z_χ . As described in Sec. IV H, one can either determine the composite operator renormalization factor Z_2 and use $Z_\chi = Z_2^2$, or evaluate Z_χ directly with the help of the perturbative correction to χ_{loc} in Fig. 4c. In both cases, the f bubble diagram is needed. To leading order in ϵ it evaluates to

$$T \sum_n G_f(i\omega_n) G_f(i\omega_n + i\nu) = \frac{|\nu|^\epsilon}{\pi\epsilon} \quad (\text{B8})$$

in the zero-temperature limit. For the correlation function $G_f^{(2,1)}$ in Fig. 4b we introduce a renormalization factor as follows: $G_f^{(2,1)} = Z_2 Z^{-1} G_{f,R}^{(2,1)}$. Demanding that the renormalized $G_{f,R}^{(2,1)}$ is free of poles at scale μ , and using $Z = 1$ we find:

$$Z_2 = 1 + \frac{u}{\pi\epsilon}, \quad (\text{B9})$$

which gives Z_χ in Eq. (45).

APPENDIX C: RG FOR THE INFINITE- U ANDERSON MODEL

The infinite- U Anderson model can be analyzed in the vicinity of $r = 1$ using an expansion in the hybridization strength. Here we describe details of the field-theoretic RG, with the results appearing in Sec. V. Starting point is the action (61), written in terms of auxiliary fields f_σ and b_s . The RG proceeds by perturbatively calculating renormalizations to the propagators and vertices appearing in (61), which yields expression for the renormalization factors defined in Eq. (66).

The relevant diagrams are displayed in Fig. 14. Note that there is no one-loop contribution to the vertex renormalization. At one-loop order we have the graphs for the f and b self-energies. Evaluation of the first diagram for the f self-energy in Fig. 14a gives:

$$(14a1) = V_0^2 T \sum_{i\omega_n} \int \frac{dk |k|^r}{i\omega_n - k} \frac{1}{i\nu - i\omega_n - \lambda_0}. \quad (\text{C1})$$

We work at criticality, i.e., $\epsilon_0 = 0$. First the frequency sum can be performed, here the $\lambda_0 \rightarrow \infty$ limit is important: it suppresses contributions from positive k . The remaining k integral is UV convergent, and we finally obtain

$$(14a1) = -\frac{V_0^2}{2\bar{r}} (i\nu - \lambda_0)^r \\ = -A_\mu \frac{v^2}{2\bar{r}} (i\nu - \lambda_0). \quad (\text{C2})$$

In the second line we have expressed the result in terms of renormalized quantities, with $A_\mu = \mu^{2\bar{r}} (i\nu - \lambda_0)^{-2\bar{r}} Z_v^2 / (Z_f Z_b)$. Demanding cancellation of poles in the expressions for the renormalized f Green's function at external frequency $i\nu - \lambda_0 = \mu$ we obtain the one-loop result for the f renormalization factor as

$$Z_f = 1 - \frac{v^2}{2\bar{r}}. \quad (\text{C3})$$

The other diagrams in Fig. 14a,b,c are evaluated in a similar manner. In the two-loop self-energies, the real part of the inner self-energy insertions, which diverges linearly with the UV cutoff, is exactly cancelled by the corresponding counter-term.

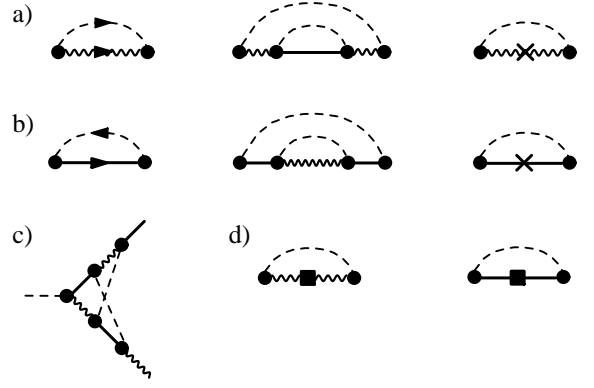


FIG. 14: Diagrams for the RG of the infinite- U Anderson model. Notations are as in Fig. 8. a),b) Self-energies for f_σ and b_s to two-loop order. The crosses denotes the counter-terms which cancel the real parts of the self-energy insertions. c) Two-loop vertex renormalization; there is no contribution to one-loop order. d) Diagrams with mass insertions (squares), needed to determine the correlation length exponent.

Collecting all expressions yields the renormalization factors, defined in Eq. (66), to two-loop order as

$$Z_f = 1 - \frac{v^2}{2\bar{r}} - \left(\frac{1}{4\bar{r}^2} + \frac{1}{2\bar{r}} \right) v^4, \\ Z_b = 1 - \frac{v^2}{\bar{r}} - \left(\frac{1}{4\bar{r}^2} + \frac{1}{2\bar{r}} \right) v^4, \\ Z_v = 1 + \frac{1}{4\bar{r}} v^4. \quad (\text{C4})$$

With these results, we can take the logarithmic μ derivative of Eq. (66) at fixed bare coupling, we obtain the beta function

$$\beta(v) \equiv \mu \frac{dv}{d\mu} \Big|_{V_0} \quad (\text{C5})$$

as quoted in Eq. (67). The anomalous field dimensions are obtained from

$$\eta_f = \mu \frac{d \ln Z_f}{d\mu} = \beta(v) \frac{d \ln Z_f}{dv} = v^2 + 2v^4 \quad (\text{C6})$$

$$\eta_b = \mu \frac{d \ln Z_b}{d\mu} = \beta(v) \frac{d \ln Z_b}{dv} = 2v^2 + 2v^4. \quad (\text{C7})$$

To determine the flow away from criticality and the correlation length exponent, we follow the standard scheme¹⁶ via insertions of composite operators, representing mass terms. Physically, only the difference between the masses of the f and b auxiliary fields is relevant, and introducing one type of composite operator is sufficient. In the following we work with $\bar{f}f$ insertions, which acquire a corresponding renormalization factor Z_{2f} . To determine Z_{2f} we consider a correlation

function $G_{bf}^{(2,1)} = \langle \langle b^\dagger(\tau)b(\tau'); (f^\dagger f)(\tau'') \rangle \rangle$. The renormalization factor Z_{2f} is then defined through

$$G_{bf}^{(2,1)} = \frac{Z_{2f}}{Z_f} Z_b G_{bf,R}^{(2,1)} \quad (\text{C8})$$

Evaluating the diagram in Fig. 14d and demanding cancellation of poles in $G_{bf,R}^{(2,1)}$ gives, to one-loop accuracy,

$$Z_{2f} = 1 + \frac{v^2}{\bar{r}}. \quad (\text{C9})$$

The correlation length exponent can be related to the Z factors via the RG equation¹⁶ for the renormalized $G_{bf}^{(2,1)}$, according to

$$\frac{1}{\nu} - 1 = \mu \frac{d}{d\mu} \ln \frac{Z_{2f}}{Z_f} \quad (\text{C10})$$

which yields

$$\frac{1}{\nu} = 1 - 3v^{*2}. \quad (\text{C11})$$

The result for ν is in Eq. (72), and is of course identical to the one obtained in Ref. 12 using the familiar momentum-shell method.

The local susceptibility exponent is determined via a renormalization factor, Z_χ , for the two-point correlations of the impurity spin. The leading diagrams are in Fig. 8c; the v^2 diagrams are identical, with a leading singular contribution of

$$\frac{1}{2} V_0^2 \int_0^\tau d\tau_2 \int_0^{\tau_2} d\tau_1 G_{c0}(\tau_2 - \tau_1) = \frac{V_0^2}{4\bar{r}} \tau^{2\bar{r}}$$

each. Note that the counter-term contributions can be ignored here, as they do not develop poles in \bar{r} . Demanding cancellation of poles yields

$$Z_\chi = 1 - \frac{v^2}{\bar{r}}. \quad (\text{C12})$$

Taking the logarithmic derivative w.r.t. μ one obtains the η_χ value quoted in Sec. VF.

The renormalization factor for the T matrix (diagrams not shown) is obtained as

$$Z_T = 1 - \frac{3v^2}{2\bar{r}} - \frac{3v^4}{2\bar{r}} \quad (\text{C13})$$

to two-loop order. The resulting anomalous exponent η_T fulfills the exact equation $\eta_T = 2\bar{r}$.

APPENDIX D: SPIN ANISOTROPIES

Thus far our discussion has been restricted to impurity models with full SU(2) spin symmetry. In this appendix we show that spin anisotropies, e.g. in the Kondo interaction, are irrelevant at all critical points considered.

For the weak-coupling RG of Sec. III A, formulated in the variables of the Kondo model, we introduce Kondo couplings J_\perp and J_z for the transverse and longitudinal part of the Kondo interaction. The RG equation (18), to one-loop order, generalizes to

$$\begin{aligned} \beta(j_\perp) &= rj_\perp - j_\perp j_z, \\ \beta(j_z) &= rj_z - j_\perp^2. \end{aligned} \quad (\text{D1})$$

For the metallic case, $r = 0$, there is a line of fixed points at $j_\perp = 0$, $j_z < 0$, representing an unscreened moment. In contrast, for $r > 0$ only SU(2) symmetric fixed points survive, namely LM with $j_\perp^* = j_z^* = 0$ and SCR with $j_\perp^* = j_z^* = r$. Thus, the symmetric critical fixed point of the Anderson and Kondo models is stable w.r.t. SU(2) symmetry breaking.

Turning to the p-h asymmetric model, we start from the infinite- U Anderson model (57) and introduce a spin dependence in the hybridization, $V_{0\uparrow} \neq V_{0\downarrow}$. As is easily seen via Schrieffer-Wolff transformation, for a generic p-h asymmetric conduction band this is equivalent to an anisotropic exchange interaction plus a local magnetic field. Without loss of generality we restrict the following analysis to a p-h symmetric conduction band, where the field term is absent. The RG equation (67), to one-loop order, generalizes to

$$\begin{aligned} \beta(v_\uparrow) &= -\bar{r}v_\uparrow + \frac{v_\uparrow}{2}(2v_\uparrow^2 + v_\downarrow^2), \\ \beta(v_\downarrow) &= -\bar{r}v_\downarrow + \frac{v_\downarrow}{2}(2v_\downarrow^2 + v_\uparrow^2). \end{aligned} \quad (\text{D2})$$

Apart from the SU(2) symmetric fixed point, $v_\sigma^{2*} = \frac{2}{3}\bar{r}$, there are two other fixed points with $v_\uparrow^{2*} = \bar{r}$, $v_\downarrow = 0$ and $v_\downarrow^{2*} = \bar{r}$, $v_\uparrow = 0$ – these are, however, infrared unstable w.r.t. finite v_\perp (v_\uparrow). Thus, the only stable critical fixed point is the SU(2) symmetric one, which corresponds to the ACR fixed point analyzed in Sec. V.

¹ A. C. Hewson, *The Kondo Problem to Heavy Fermions*, Cambridge University Press, Cambridge (1997).

² D. Withoff and E. Fradkin, Phys. Rev. Lett. **64**, 1835 (1990).

³ C. R. Cassanello and E. Fradkin, Phys. Rev. B **53**, 15079 (1996) and **56**, 11246 (1997).

⁴ A. Polkovnikov, Phys. Rev. B **65**, 064503 (2002).

⁵ R. Bulla, T. Pruschke, and A. C. Hewson, J. Phys.: Con-

- dens. Matter **9**, 10463 (1997); R. Bulla, M. T. Glossop, D. E. Logan, and T. Pruschke, *ibid* **12**, 4899 (2000).
- ⁶ C. Gonzalez-Buxton and K. Ingersent, Phys. Rev. B **57**, 14254 (1998).
 - ⁷ K. Ingersent and Q. Si, Phys. Rev. Lett. **89**, 076403 (2002).
 - ⁸ D. E. Logan and M. T. Glossop, J. Phys.: Condens. Matter **12**, 985 (2000).
 - ⁹ J. Bobroff, W. A. MacFarlane, H. Alloul, P. Mendels, N. Blanchard, G. Collin, and J.-F. Marucco, Phys. Rev. Lett. **83**, 4381 (1999).
 - ¹⁰ J. Bobroff, H. Alloul, W. A. MacFarlane, P. Mendels, N. Blanchard, G. Collin, and J.-F. Marucco, Phys. Rev. Lett. **86**, 4116 (2001).
 - ¹¹ See e.g. J. J. Binney, H. J. Dowrick, A. J. Fisher, and M. E. J. Newman, *The Theory Of Critical Phenomena*, Oxford University Press, Oxford (2002).
 - ¹² M. Vojta and L. Fritz, cond-mat/0309262.
 - ¹³ F. D. M. Haldane, Phys. Rev. Lett. **40**, 416 (1978).
 - ¹⁴ A. J. Leggett, S. Chakravarty, A.T. Dorsey, M.P.A. Fisher, A. Garg, and W. Zwerger, Rev. Mod. Phys. **59**, 1 (1987).
 - ¹⁵ R. Bulla, N. Tong, and M. Vojta, Phys. Rev. Lett. **91**, 170601 (2003).
 - ¹⁶ E. Brezin, J.C. Le Guillou, and J. Zinn-Justin, in *Phase transitions and critical phenomena*, eds. C. Domb and M. S. Green, Page Bros., Norwich (1996), Vol. 6.
 - ¹⁷ M. Vojta, C. Buragohain and S. Sachdev, Phys. Rev. B **61**, 15152 (2000).
 - ¹⁸ S. Sachdev, Phys. Rev. B **55**, 142 (1997).
 - ¹⁹ S. Sachdev, C. Buragohain and M. Vojta, Science **286**, 2479 (1999)
 - ²⁰ S. Sachdev, *Quantum Phase Transitions*, Cambridge University Press, Cambridge (1999).
 - ²¹ I. Affleck and A. W. W. Ludwig, Phys. Rev. Lett. **67**, 161 (1991), Phys. Rev. B **48**, 7297 (1993).
 - ²² S. Florens and A. Rosch, Phys. Rev. Lett. **92**, 216601 (2004).
 - ²³ M. Vojta and R. Bulla, Phys. Rev. B **65**, 014511 (2002).
 - ²⁴ E. W. Hudson, S. H. Pan, A. K. Gupta, K. W. Ng, and J. C. Davis, Science **285**, 88 (1999); S. H. Pan, E. W. Hudson, K. M. Lang, H. Eisaki, S. Uchida, and J. C. Davis, Nature **403**, 746 (2000).
 - ²⁵ A. Polkovnikov *et al.*, Phys. Rev. Lett. **86**, 296 (2001).
 - ²⁶ M. Kirčan and M. Vojta, Phys. Rev. B **69**, 174421 (2004).
 - ²⁷ P. W. Anderson, J. Phys. C **3**, 2436 (1970).
 - ²⁸ M. Vojta and M. Kirčan, Phys. Rev. Lett. **90**, 157203 (2003).
 - ²⁹ A. Zawadowski and P. Fazekas, Z. Physik **226**, 235 (1969); P. Coleman, Phys. Rev. B **29**, 3035 (1984).
 - ³⁰ T. A. Costi, J. Kroha, and P. Wölfle, Phys. Rev. B **53**, 1850 (1996).
 - ³¹ J. Zinn-Justin, *Quantum Field Theory and Critical Phenomena*, Clarendon Press, Oxford (2002).
 - ³² S. Pankov, S. Florens, A. Georges, G. Kotliar, and S. Sachdev, Phys. Rev. B **69**, 054426 (2004).
 - ³³ M. T. Glossop and D. E. Logan, J. Phys.: Condens. Matter **15**, 7519 (2003).
 - ³⁴ K. Chen and C. Jayaprakash, Phys. Rev. B **57**, 5225 (1998).
 - ³⁵ K. Satori, H. Shiba, O. Sakai, and Y. Shimizu, J. Phys. Soc. Jpn. **61**, 3443 (1992).
 - ³⁶ W. Metzner and D. Vollhardt, Phys. Rev. Lett. **62**, 324 (1989); A. Georges, G. Kotliar, W. Krauth, and M. J. Rozenberg, Rev. Mod. Phys. **68**, 13 (1996).
 - ³⁷ Q. Si, S. Rabello, K. Ingersent, and J. L. Smith, Nature **413**, 804 (2001) and Phys. Rev. B **68**, 115103 (2003).